ADVANCED LASER DIAGNOSTICS FOR CHARACTERIZATION OF PARTICLE FLOW FIELD AND CHEMICAL SPECIES DURING ENERGETIC MATERIAL REACTIONS

A Thesis

by

NICHOLAS ANTHONY NIEMIEC

Submitted to the Office of Graduate and Professional Studies of
Texas A&M University
in partial fulfillment of the requirements for the degree of

MASTER OF SCIENCE

Chair of Committee,	Waruna Kulatilaka
Committee Members,	Eric Petersen
	Chad Mashuga
Head of Department,	Andreas Polycarpou

August 2018

Major Subject: Mechanical Engineering

ABSTRACT

Inhaling air-borne metal particles is known to cause adverse health effects such as cancer, pulmonary heart disease, and asthma, to name a few. Metal particles can be released to air from various additives often used to produce desired combustion characteristics of propellants, pyrotechnics and explosives. The focus of the present study is to characterize the release of metals during energetic reaction of defense-related explosive compounds. Evaluation of health effects and deriving proper mitigation strategies require in-situ diagnostic methods of measuring the concentration of metal particles within the flame zone of an explosive material reaction. The experiments described here characterize those metal particles, as well as their flow pattern, in the vicinity of the flame zone. Propellant strands are used to create a controlled flame zone for study, with each strand containing varying amounts of concentration of different metals of interest. High-speed digital in-line holography (DIH) is used to quantify particle size, particle velocity, three-dimensional location within the flame zone, and the density of particles within the region of interest. Under current experimental conditions, the particles imaged were found to be 100–200 microns, with an average velocity of 3 m/s. As the particles ejected spread out in different directions, the spatial location closest to the strand contains the highest density of particles. The chemical composition, specifically the type of metal concentration of the ejected particles is observed through a simultaneous laser-induced breakdown spectroscopy (LIBS) experimental system. The spectrally resolved emission following a localized plasma generated using an intense nanosecond-

duration LIBS laser pulse reveals specific metal type and relative concentration. To the best of our knowledge, the present work demonstrates simultaneous particle flow-field characterization and metal speciation using combined DIH and LIBS techniques, in a gas-phase reacting flow field.

DEDICATION

I dedicate this work to my wife, Chelsea, for her constant devotion and support she has shown me.

ACKNOWLEDGEMENTS

I would like to thank my committee chair, Dr. Waruna Kulatilaka, and my committee members, Dr. Eric Petersen and Dr. Chad Mashuga for their guidance and support throughout the course of this research.

Thanks also go to my friends and colleagues and the department faculty and staff for making my time at Texas A&M University a great experience.

Lastly, I cannot have accomplished my work without the help of family. Thanks go to my mother and father for their guidance in my path to college and being my support and to my sister, Kelly, who always made time to listen to my concerns and provide encouragement.

CONTRIBUTORS AND FUNDING SOURCES

Contributors

This work was supervised by a thesis committee consisting of Dr. Waruna Kulatilaka and Dr. Eric Petersen of the Department of Mechanical Engineering and Dr. Chad Mashuga of the Department of Chemical Engineering.

All work for the thesis was completed by the student, in collaboration with Tyler Paschal, Ayobami Shoyinka, Pradeep Parajuli, Yejun Wang, Ayush Jain, and Catherine Dillier of the Department of Mechanical Engineering.

Funding Sources

This research activities described here were funded by a grant from the Department of Defense (DoD) Strategic Environmental Research and Development Program (SERDP). The author was supported by a graduate research assistantship under the same program.

The contents are solely the responsibility of the authors and do not necessarily represent the official views of SERDP.

TABLE OF CONTENTS

Page

LIST OF FIGURES

Page

1. INTRODUCTION

1.1 Background

Energetic materials are compounds that release energy quickly, either to make use of the energy released or the heat released. These materials can be the basis of explosives, propellants, ammunition, or even pyrotechnics [1]. Depending on the application for the material, different combustion parameters are desired. Metal particulates, most often aluminum, are added to propellant materials to produce desired characteristics. In ammunition powder, for example, aluminum particles can be added to raise the reaction temperature, enhance the air blast, and increase the heat of detonation [1]. The solid rocket boosters of NASA's space shuttle utilize aluminum powder as the fuel in the propellant [2]. In any application, the added metal particulates are ejected into the atmosphere during combustion. This can be concerning in cases where humans are in close proximity to the combustion products. The inhalation of metal particulates, whether aluminum or some other metal is known to cause adverse health effects such as cancer, pulmonary heart disease, and asthma [3]. In order to conduct future health-related studies, it is vital to first understand metal particle combustion in these scenarios.

Laser inducted breakdown spectroscopy (LIBS) is the technique proposed to conduct these concentration measurements. Figure 1 shows a basic LIBS apparatus.

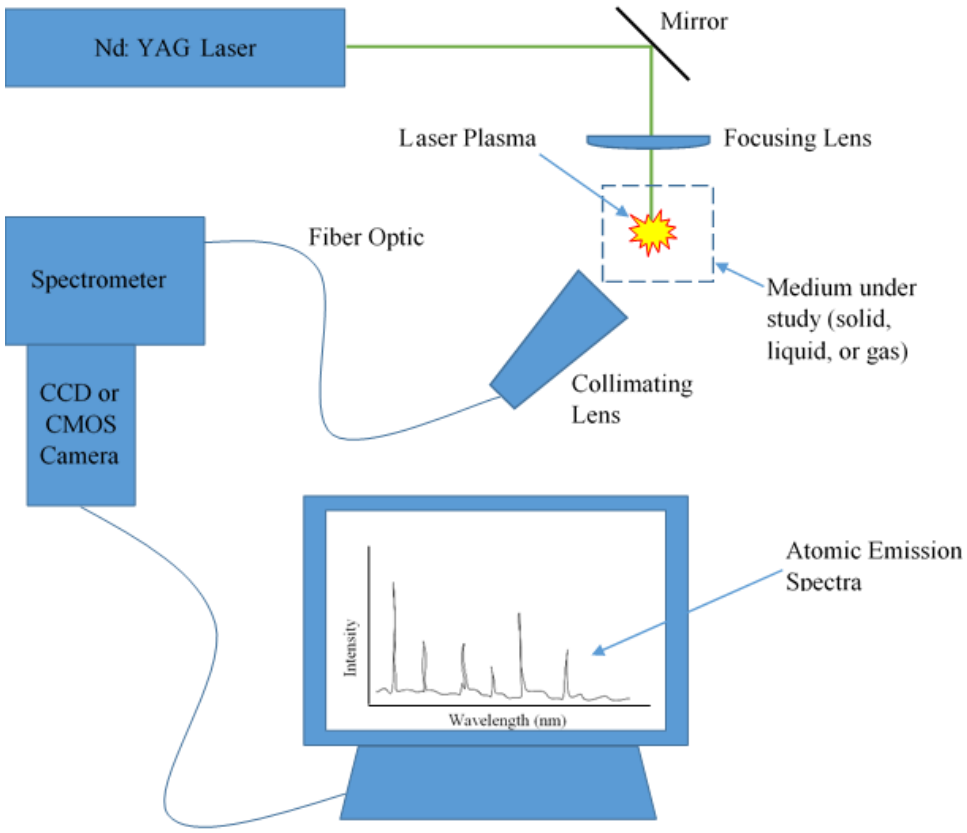

Figure 1. Example LIBS experimental apparatus and a sample spectrum.

In LIBS, a laser beam is focused to a small point. At this point, the beam irradiance is increased so much that a small plasma is formed out of the material at the focal point [4]. A solid, liquid, or gas material will still form a plasma. This plasma contains information about all of the basic elemental species of the materials present. These atoms are excited to higher energy states and as they fall back down, they emit light at a characteristic wavelength. This light can then be captured with a spectrometer, which determines the elements within the light [4]. The computer in Figure 1 shows the spectrum

of light that is captured with the setup. Using LIBS, the intensity of light captured can then be correlated to the concentration of the element found. Early experiments showing the possibility of using nanosecond Nd: YAG lasers to measure concentrations of metal particles within combustion flames have already been conducted by my colleague and can be found in his literature [5].

One of the primary questions resulting from this previous research is "*why 10-Hz nanosecond LIBS only sometimes collects characteristic signals, whereas 1-kHz femtosecond LIBS measurements resulted in species-specific emission lines at almost every laser shot?"* To answer this question, the present study is planned to quantify the following information about the particles: diameter, velocity, spatial location, and density, as well as the chemical composition, simultaneously. An improved understanding of metal particle combustion can lead to the successful implementation of LIBS techniques for quantitative concentration studies of detecting metal particles in realistic practical environments.

1.2 Significance of the Thesis Research

The United States Army is especially interested in understanding how post-combustion products affect health, specifically the inhalation of metal particulates. Operators who are in close proximity to the products of combustion of weapons are at particular risk for obtaining some adverse health effects. The techniques that are proposed for study in this thesis are well researched and documented laser diagnostics. LIBS has been making significant strides towards a more universal laser diagnostic method. DIH is an emerging technique that has been gaining ground since the advent of high-speed

imaging hardware and high-processing-power computers. With typical holography experiments collecting tens of thousands of frames, processing requires intense algorithms that can take days to complete [6].

The goal of the work in this thesis is to try and combine these laser diagnostics into one experiment. DIH allows for the detection of particle sizing, velocity, and distribution, and coupled with LIBS, the chemical composition of these particles can be verified. As with any exploratory research, this can be a daunting task. Taking two well-known diagnostics and putting them together does not necessarily mean that everything will work the first time. Rather, this thesis shows promise of utilizing these laser diagnostics together and provides a basis for future experiments.

1.3 Thesis Outline

The main laser diagnostics used to determine the concentration of metal particulates within the combustion flame are LIBS and DIH. A significant background and literature review for these tools are presented in Section 2. Section 2 also details the reason metal powders, such as aluminum, are used in propellants and why nanoparticles adversely affect health. An overview of the experimental apparatus and procedures used for the detection of these particulates is covered in Section 3. The results from these experiments are presented in Section 4, combined with a discussion of the results. Section 5 contains concluding remarks and recommendations for future work.

2. LITERATURE REVIEW

2.1 Background on Propellants

2.1.1 Brief History of Propellants

It is hard to pinpoint the moment when propellants first starting being used by humans on this planet. In order to better understand the first uses of solid propellants in history, a definition of what they are should be stated. Propellants are chemicals that release huge amounts of gaseous products, at high temperature and pressure, in a rapid amount of time. Solid propellants often contain an oxidizer, fuel, binder, plasticizer, curing agent, stabilizer, and a cross-linking agent [7]. Depending on the end use of the propellant, different chemical constituents can be used for each of these ingredients. It is the high-pressure gases that are then used to propel rockets, missiles, and projectiles. It is important to note that propellants are different than fuels. A propellant is a mixture that actually contains both a fuel and an oxidizer. Because both the fuel and the oxidizer are present in the mixture, it can be difficult, if not impossible, to stop the combustion process once it has begun. Some of the first uses of propellants that are recorded in history include Greek fire in the 7th century by Byzantine defenders, followed by uses of black powder used to propel stones by Muslims in the 13th century [8]. In the 20th century, the advancement in the technology of conventional weapons was fast. There were many types of rapid-fire weapons, recoilless weapons, and rockets and missiles that all used combustion gases from propellants to launch projectiles. Many of these weapons, though, were operated in enclosed spaces. It is hard to replicate exposures such as these in field conditions, and therefore it is hard to conduct studies on health-related effects.

Kirchner in *Combustion Products of Propellants and Ammunition* provides a very good overview of the use and history of propellants, and also ties in their adverse health related effects [8]. Specifically, the adverse exposures that are mentioned include the combustion products of propellants and other chemicals, the materials that make up the projectile being fired, and the materials that are ejected due to the interaction between the projectile and the firing barrel [8]. One preliminary study was found that was conducted in an effort to correlate health-related effects to the inhalation of combustion products from ammunition propellant [9]. The study proved promising, however, it calls for more in-depth studies to be conducted in the future.

2.1.2 Propellants and Metal Additives

In the present age, the use of solid propellants remains primarily for gun and rocket propulsion. Solid propellants excel at these applications due to their ability to create high temperature gaseous products from combustion. Depending on the specific application, the chemical composition can vary from one propellant to another, providing different combustion characteristics for each propellant. Over the last century, AP/HTPB type propellants have been used extensively. During this time period, testing was conducted heavily on the specific chemical constituents added to propellants. Metal powders, such as aluminum, became a common addition. Aluminum powder has been added as small particles, on the order of 5-60 μm, and can comprise 14-20% of the propellant mixture by weight. It was found that the addition of aluminum on this scale improved the heat of combustion, propellant density, combustion temperature, and, due to increases in all of these, the specific impulse [10].

Due to the enhancements that metal powders add to solid propellants, metal nanoparticles have also been studied as energetic additions to propellants. Energetic materials that are often used include monomolecular compounds, such as TNT and RDX. The heat of combustion of these material types are usually limited by the enthalpy of formation of their reaction products. These monomolecular materials are used because their exothermic reactions occur very rapidly; however, the energy densities of these materials are relatively low. This is where metal-based fuels are important. Combusting metal particles, such as aluminum, allows for higher combustion energies to be obtained, and through this, higher energy densities. Albeit, the cons of using metal particles is because of their relatively low rates of energy release. The ignition of micron-sized particles is rather slow compared to monomolecular energetic compounds. Another issue is the agglomeration of unignited aluminum particles. Large metal particle agglomerates may never ignite, or only ignite after long delay times. This results in a decreased efficiency of the propulsion system and the specific impulse obtained from the combustion of the propellant. Due to these downsides, research points towards using smaller particles with higher specific area. This would lead to smaller ignition delays. The wide-spread testing of nanosized aluminum powders seems to come from the conventional use of aluminum particles widely used in explosives and propellants [11].

2.1.3 Increasingly Smaller Metal Particles

Nanoparticles first started seeing potential applications in optical, electrical catalytic, and magnetic type fields of study. As a particle decreases in size, it starts to gain interesting properties, namely a large specific surface area. Therefore, nanometal powders seem to have promising effects for propellants due to their high reactive abilities [12].

Arkhipov (2011) conducted studies on the ignitability of composite solid rocket propellants with varying aluminum powder sizes using a CO2 laser in atmospheric conditions [13]. The interest in varying the size of metal powders came over the last century of additive testing. Conventional composite solid propellants contained micron-sized aluminum powders, with powders on the order of 3-20 μm. Current technology allows for the production of ultrafine metal powders, with particle sizes on the order of ~0.1 μm. This allows for metal powders with controlled properties and high stability. It was found that the use of ultrafine aluminum powder leads to a reduction in ignition time [13].

Luca (2005) also studied the effect of varying aluminum particle size on ballistic characteristics of composite solid rocket propellants. According to the study, metal particles on the nano-scale show improvement over current ballistic performance. Two of the key factors that are enhanced include the density and specific impulse. Nano-aluminum allow for faster steady burning rates compared to micro-aluminum counterparts, mainly due to the increased specific surface area and finer dispersion of nano-powders. Specifically, with increased surface area comes an increase in reactivity. Despite these advancements, the authors did note shortcomings of nano-powders,

including safety hazards [14]. Pang (2016) used SEM and laser granulometry diagnostic techniques to study the effect of aluminum particle sizing on the combustion performance of fuel rich solid rocket propellants. Reactive metal powders have the ability to affect the specific impulse of solid propellants, with varying impacts based on particle size. It was found that the heat of combustion increased with increasing mass fraction of nAl powder [15].

The advancements of nanoparticle additions to solid propellants is now going in a new direction. Sossi (2013) studied the effect of coating nano-aluminum particles on ballistic characteristics compared to non-coated nano-aluminum formulations. It is already known that the regression rate of solid fuels can be increased by mixing metal nanoparticles into the propellant. From the literature, nanoparticles have an apparent advantage in improving combustion ballistics due to the burning surface. Increasing the surface area helps the effects of radiation and high enthalpy release closer to the burning surface. The downside is that metal nanoparticles, such as nAl, oxidize significantly during storage due to high reactivity. These studies proved promising, with some of the coating formulations showing increased regression rates. However, the authors note that further experimental work is needed to fully characterize the effects of these coatings on ballistic behavior [16].

2.2 Health Effects Surrounding Solid Propellants

2.2.1 Health Effects of Small Arms Weapons

The main cause of concern surrounding propellant ammunition over the last century has been lead. Lead was mainly used as the projectile being shot out of a weapon.

Significant environmental and health testing, however, uncovered the adverse health effects surrounding lead. Pushes were thus made to redesign ammunition with different materials. One research study points out, though, that environmental and health testing has not been conducted on humans surrounding newer unleaded ammunitions [9].

That study was a Norwegian study published in 2014 was the first to conduct an initial study on unleaded ammunitions. The study goal was set in motion due to Norwegian soldiers reporting health related symptoms after live-firing with an HK416 rifle. The study therefore used the HK416 rifle but studied three different types of ammunition – a leaded, unleaded, and modified unleaded version. Fifty-five men from the Norwegian Army took part in the study. The criteria to become a member of the study required the men to be non-smokers, have no health-related symptoms such as obstructive pulmonary disease, allergies, and asthma four weeks prior to the study, and no exposure to fumes from firing live ammunition two weeks prior to the study [9].

The 55 men were randomly divided into three groups, each group being designated with one of the three types of ammunition studied. The group, however, had no knowledge of the type of ammunition they were firing. The tests involved a participant being placed inside of a semi-airtight tent. The subject laid down suppose pose and had a CO meter placed near their mouth. This meter measured the CO concentration inside the tent, and also levels of COHb from the subject. The subject was instructed to fire one round at a time, and to not fire a successive round until the concentration level of CO inside the tent fell below 200 ppm. Measuring the amount of COHb that came from the test subject

helped to determine whether health-related symptoms were coming from the toxic presence of CO [9].

Solid particulates from combustion were collected via a 0.4-micron polycarbonate filter. An internal standard was applied to the filters such that testing with an ICP-MS could verify correct measurements. The filters were then tested for Cu, Zn, Pb, Sn, and Bi. In terms of recording symptoms, subjects were required to fill out a questionnaire immediately after the trial, and then again after 24 hours. The questionnaire asked questions about general symptoms, and then about respiratory specific symptoms. It is important to note that in these studies, Copper was the metal present more than any other, with a concentration of 5.4 mg/m^3. The American Conference of Governmental Industrial Hygienists delineate a threshold limit value at 0.2 mg/m3. Despite these high levels of Copper, statistical procedure shows no relation between different variables and symptoms. Using a principal component analysis, it shows that most of the symptoms seen by subjects have some relation to CO. However, the levels of COHb measured from the subjects were not high enough to be able to clearly link CO as the main cause of health-related symptoms. Rather, it is thought that particle size might be a concern. The study did not conduct any analysis into the sizing of particles. The research does, though, clearly call for future research into chemical and physical classification of the combustion products, including particle sizing and distribution [9].

2.2.2 Nano-Particulates and Health

As a new and emerging field, nanotechnology presents many important aspects. Solid propellants have been evolving slowly over the last century, and nanoparticles are

being tested at growing rates for their ability to produce desired combustion effects. Alongside this push, there are some researchers studying the effect of nanoparticles on human health. Nanoparticles are particles that have diameters of 100 nm or less. Small particles larger than this are classified as particulates and are grouped into groups based on their size. Nanoparticles have been shown to cause asthma and cardiovascular disease [3].

Metal particulates within combustion can occur from metal particulates that are intentionally placed within the propellant. Lead was a metal that used to be very important for ballistic design. As combustion of the ammunition propellant propelled the projectile out of the gun barrel, lead and products of reaction from lead such as lead monoxide helped to create a lubrication effect that protected the gun barrel [17]. The replacements of lead included steel, and other strong metals like tungsten and tungsten alloys [17]. However, as harder metals pass through gun barrels without lubrication, abrasion necessarily occurs. This contributes to a certain amount of the metal particulates that are found in combustion products of ammunition propellants. These include metal particles of lead, copper, and zinc [17]. It is important to note that the inhalation of metal particulates can cause chronic health problems [17]. Specifically, for example, breathing in of copper particulates has been documented to cause nasal congestion, nasal septum perforation, nasal ulceration, and metal fume fever [17]. In the health community, nanoparticle testing is being done via in vitro and animal studies. It has been shown that nanoparticles have the ability to cause inflammation, allergies, autoimmune diseases, and even cardiorespiratory effects [3].

Research has shown that one of the main reasons why nanoparticles have such an adverse effect on biological systems is their size. Same chemical materials, but that are on the bulk scale size do not have the same physicochemical properties as their nanoparticle cousins. Surface area seems to be one of the biggest issues. With increased surface area, nanoparticles have more atoms and molecules on their surface as compared to the inside of the particle. These small particles can therefore disrupt biological systems at the cellular, subcellular, and protein levels [18].

2.3 Fundamentals of LIBS

2.3.1 Background on LIBS

Laser-induced breakdown spectroscopy stemmed from the introduction of the laser in the 1960s. LIBS is actually a type of atomic emission spectroscopy (AES). AES is a technique that has the ability to determine the elemental composition of a sample under study. This sample can be in either the solid, liquid, or gaseous phase. In any case, the atomization of a sample causes free electrons and ions to be created. As the atoms are excited to higher energy states, they fall back down while emitting light. This light is characteristic of the specific elements that were excited. By analyzing the spectra of light collected from these plasmas created from atomic emission, the elements can be characterized, and the intensity of light collected can be related to concentration. AES techniques have been around since the middle of the 19th century. Typical methods have used electrode arcs and sparks, inductively coupled plasmas, direct coupled plasmas, microwave induced plasmas, and hollow cathode tubes in order to promote the atomization and vaporization of samples. A drawback to some of these techniques,

however, is that they require extensive laboratory setups. On the contrary, LIBS is a simple technique that can be conducted with little to no setup. LIBS can be conducted in all environments and is non-invasive. It produces spectra almost instantaneously, allowing for in situ measurements. Lastly, while AES is an elemental analysis, LIBS can be used for molecular species identification as well with the use of high resolution, broadband spectrometers [4, 19].

LIBS uses a high powered, focused laser pulse to create a vaporizing plasma. The laser pulse is focused using a focusing lens to the specific location where the laser irradiance is increased to a level required for sample breakdown. The resulting plasma light that is emitted is then collected using a collimating lens and fiber optic. Figure 1 shows an example LIBS setup. An Nd: YAG (neodymium yttrium aluminum garnet) laser is a common laser used for LIBS studies. Common laser wavelengths used include 532 nm and 1064 nm, at a rate of 10 Hz. This laser pulse can then be guided to the sample under study with mirrors and focused with a focusing lens. The collimating lens collects the light from the plasma and guides it to a spectrometer with a fiber optic cable. Once inside the spectrometer, the collected light is expanded out using a grating. Light can then be passed on to the CCD or CMOS camera chip [4, 19].

2.3.2 LIBS in Literature

Laser induced breakdown spectroscopy has been a commonly used diagnostic for several decades. Moench (1997) describes the use of laser induced breakdown spectroscopy for the characterization of metal additives to polymers [20]. Le Drogoff (2004) demonstrates the effect of laser pulse duration on the signal achieved by laser

induced breakdown spectroscopy of solids [21]. Cheng (1999) studied the ability of laser induced breakdown spectroscopy to be used to study particles in the gas phase and aerosols [22]. Their experiments showed that the LIBS technique needed to be augmented in order to detect trace metals. By enhancing their LIBS measurements with an aerosol beam-focusing device, they were able increase their measurement sensitivity. Cheng (1999) studied the ability of laser induced breakdown spectroscopy to be used to study particles in the gas phase and aerosols. Their experiments showed that the LIBS technique needed to be augmented in order to detect trace metals. By enhancing their LIBS measurements with an aerosol beam-focusing device, they were able to increase their measurement sensitivity. Vander Wal (1999) presented an alternate method to detecting trace metals in liquids [23]. Instead of performing laser induced breakdown spectroscopy on the liquid medium itself, Vander Wal deposited their liquid onto a carbon planchet, whereupon the liquid evaporated. This method effectively changes a liquid LIBS setup into a solid LIBS setup [23]. Fichet (2000) studied the ability of LIBS to be conducted in two different types of liquid media – water and then oil. Their experiments showed an ability to have detection limits of 0.3 to 120 μg/ml, with a reproducibility of 3% [24].

Ferioli (2005) studied the use of laser induced breakdown spectroscopy to determine equivalence ratios for propane and methane in air [25]. Kim (2017) showed an advanced system of laser induced spectroscopy where a plug that is placed within the piston-cylinder chamber can conduct species analysis. This helps to determine the equivalence ratio in the chemical reaction zone instantaneously [26]. Rezaei (2016) studied the ability for laser induced breakdown spectroscopy to determine the aluminum

content within RDX-based explosives, and the effect of aluminum percentage on combustion performance [1]. Zhang (2014) studied the use of laser induced breakdown spectroscopy to study nanoparticle volume fraction within combustion flames [27]. The authors modified the conventional LIBS approach by lowering the intensity of the laser beam. Conventional LIBS results in a plasma on the order of millimeters that breaks down all molecules that are in the area. By lowering the laser energy, so called phase-selective LIBS is able to detect the specific particles under study, TiO2 nanoparticles [27]. Lee (2005) demonstrates the ability of laser induced breakdown spectroscopy to study temperature of combustion flames [28].

2.3.3 Related Previous Work within Our Group

Papers written by O'Neil are a good background to the work presented in this thesis [5, 29, 30]. The work studied in this thesis was the future work section outlined in those papers. The purpose of the work by O'Neil was to determine if LIBS is a good diagnostic for characterizing the emissions of explosive materials. Specifically, measuring the concentration of metal particles such as aluminum, copper, mercury and lead in the surrounding air after combustion of ammunition propellants is important. The work in O'Neil (2017) shows promise in the ability to create a correlation between the LIBS intensity signal and the concentration of metal particles within the products of combustion.

LIBS is a technique that has been used extensively on solids, with research now pushing for more of its use in liquids and gases. LIBS has also been used in aerosols and detecting particles in combustion flames.

In this study, the combustion of ammunition propellant was modeled by burning solid propellant strands. Before studying the solid propellant strands with LIBS, however, numerous preliminary studies were conducted. These included studying solid metal plates to calibrate the LIBS system, a laser energy study to determine an appropriate level of energy that did not create too much noise, and a plasma decay study to determine the best gating time to use. After these initial studies, solid propellant strands were then studied. The LIBS signal for the different metal powders studied were much weaker than the signals achieved when studying solid metal plates. This is most likely due to the small number density of metal particles that are found within the flame. Also, as the solid propellant strand burned down, the LIBS signal was kept stationary. Therefore, particles that are ejected from the propellant strand are moving in all different directions and may or may not have a trajectory that runs into the LIBS signal. Despite these shortcomings, experiments using propellant strands with aluminum particles added were able to detect metal aluminum particles, and a promising concentration calibration curve was able to be created. Signals of the other metals – copper, lead stearate, and mercury chloride – were not able to be detected. Because of this, more characterization of the particles being ejected from the solid propellant strands is desired [5, 29, 30].

2.4 Fundamentals of Digital In-line Holography (DIH)

2.4.1 Background to Holography

Adrian (1991) provides a review of techniques used for measuring information about particles. Determining velocity vectors about particles, and thus learning how particles are moving within flows, is especially important. Some of the modern techniques

that are available for conducting these measurements include particle image velocimetry (PIV), molecular tracking velocimetry, particle tracking velocimetry (PTV), laser speckle velocimetry, planar laser-induced fluorescence (PLIF), and nuclear magnetic resonance imaging. These techniques use markers to track how particles are moving within a specific flow field. Pulsed laser light is then used to visually record these markers at different instances in the flow field, recording the images either on photography film, a CCD or CMOS sensor, or holographic film [31].

Katz (2009) provides a review of the status of holographic velocimetry [32]. This review is a great introduction and background to the fundamental aspects of holography, as well as the mathematical background of numerical reconstruction. Holography was first thought of by Dr. Dennis Gabor in 1948. Specifically, Dr. Gabor was trying to employ wave-front reconstruction as a method for increasing resolution of microscopy. Despite his initial insights, it was not until the advent of the laser in the early 1960s that holography was a viable technique. Holography began in an analog format, where holograms were recorded with specially designed holographic film. A simple diagram outlining the idea behind holography is shown in Figure 2. First, a laser produces light that is coherent and has minimal divergence. This light is then divided into two separate beams: a reference beam, and an object beam. The object beam illuminates the object that is being studied. In the example shown, the objects are small particles in a flow field. The reference beam does not illuminate the object field, but rather illuminates the holography film. The key to the technique is that the object beam that illuminates the object field diffracts off of the objects under study. This diffracted light then interferes with the reference beam.

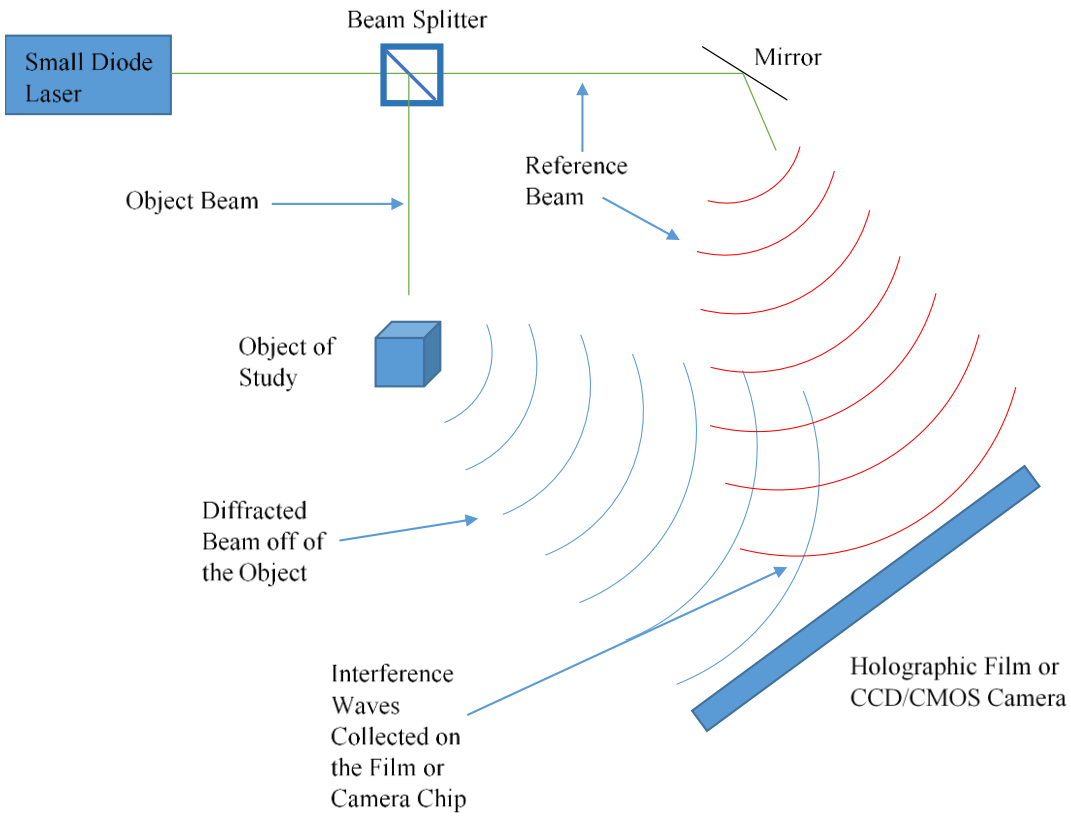

Figure 2. Schematic of a holography experiment.

Therefore, the light that is captured on the holographic film is an interference pattern between the reference beam and the diffracted object beam. This is a 2D pattern encoded on the film; however, it reveals information about the amplitude as well as the phase of the diffracted waves. Figure 3 shows a magnified, side-angle view of this holographic film with the encoded pattern on it.

(A) (B)

Figure 3. Schematic showing the side angle of a holographic film. (A) Holographic film that has not been exposed yet. (B) Holographic film that has been exposed.

Reconstruction of the object field that was studied is possible when this holographic film is re-illuminated with a reference beam that impinges the film at the same angle the initial reference beam used. The reference beam diffracts through the pattern on the film and creates the object field that was previously captured during the experiment. Figure 4 demonstrates this reconstruction process.

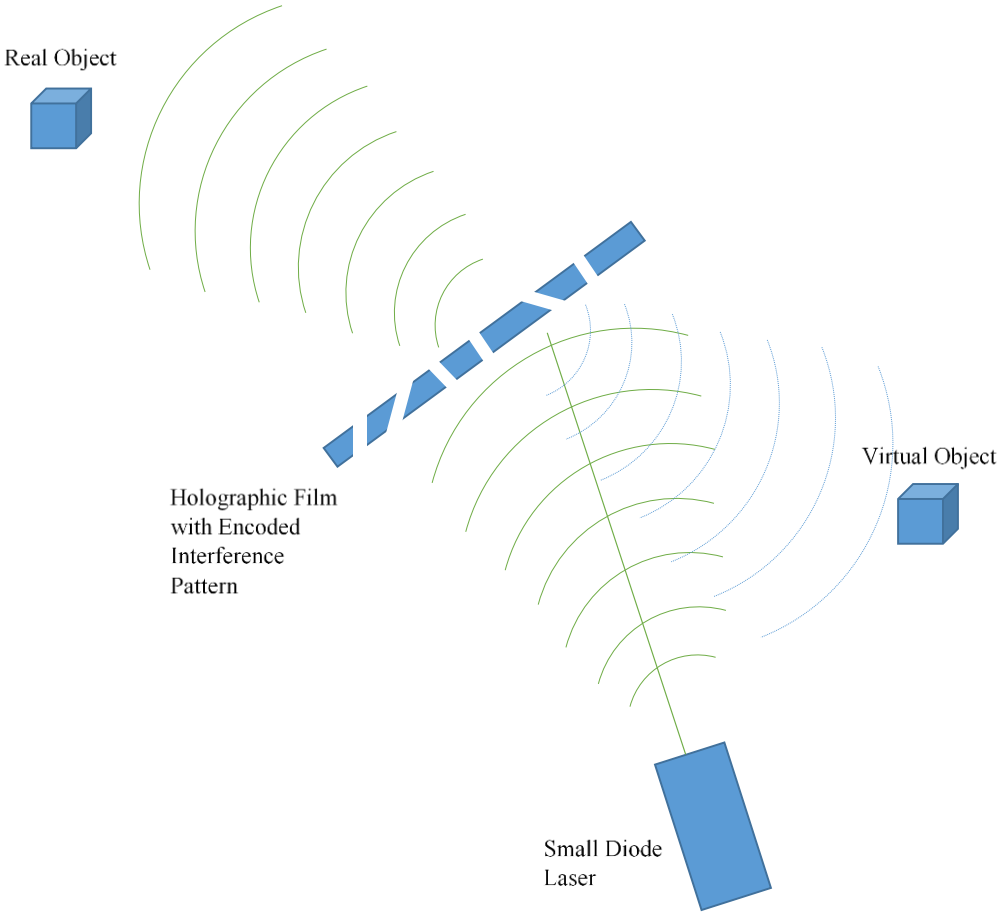

Figure 4. Analog holography reconstruction schematic.

Modern technology is allowing for the advancement of holographic techniques. Digital holography allows for easier experimental procedures; however, the analysis of data becomes a key factor in determining the feasibility of the technique. It should be noted that holography experiments differ in how the initial reference and object beams relate to each other. If the beams are parallel, the setup is termed “in-line holography”. If those beams are not parallel, the setup is termed “off-axis holography”.

One of the major problems that has always faced holography is termed the depth-of-focus (DOF) problem. The fact that holography, and any imaging system, has a finite aperture means that the resolution of a reconstructed image and the depth space where objects are able to be focused are both limited. It has been shown that the measurement uncertainty of the axial location, or depth location, of particles is related to d/λ. There are many papers that show how to reduce the uncertainty, whether for analog or digital holography [32].

2.4.2 Mathematical Basis of Reconstruction

There are several sources that outline the mathematics behind holography recording and reconstruction [32, 33]. The first step is modeling the light that illuminates the holography film or sensor array. This light is the interference pattern between the reference wave R and the object wave O, and is merely the intensity of this light, represented by:

$$I_h(x_h, y_h) = \left(\tilde{R} + \tilde{O}\right)\left(\widetilde{R^*} + \widetilde{O^*}\right) = RR^* + \tilde{R}\widetilde{O^*} + \widetilde{R^*}\tilde{O} + \tilde{O}\widetilde{O^*}$$

I_h represents the amplitude of the hologram at any given x/y location on the film or sensor. The asterisk (*) in this equation represents the complex conjugate of the specific wave, whether R or O. On the right-hand side of this equation, the first term represents the mean irradiance of the beam, the second and third terms represent the interference patterns, and the fourth term relates to noise. Analog reconstruction of a hologram incorporates taking a reference beam and illuminating the film. This reference wave goes through the film and

diffracts through the interference pattern captured on the film, creating the 3D image that was captured during the experiment. A similar methodology is used during digital reconstruction. A reconstructed image is recreated by multiplying a conjugate reference wave with the hologram interference pattern:

$$\widetilde{U_r} = \widetilde{R^*} I_h = \|R\|^2 R^* + \|R\|^2 \widetilde{O^*} + \widetilde{R^{*2}} \tilde{O} + R^* \tilde{O} \widetilde{O^*}$$

On the right-hand side of this equation, the first term represents the reference wave, the second term is the reconstructed real image, the third term is the reconstructed virtual image, and the fourth term is the reference beam affected by the halo noise. Taking this theory, algorithms represent the reference beam diffracting through this "digital film", creating the optical field known as the digitally reconstructed hologram:

$$\widetilde{U_r}(x, y, z) = \iint_{x_h \, , \, y_h} \widetilde{U_r}(\xi, \eta, z = 0) \left[-\frac{\partial G}{\partial n}(x - \xi, y - \eta, z) \right] d\xi d\eta$$

In this equation, $\partial G/\partial n$ is the normal derivative of Green's function and is computed either by the Rayleigh-Sommerfeld formula, or the Kirchhoff-Fresnel approximation. In either case, this whole formula is most frequently calculated in the frequency domain through the equation:

$$\widetilde{U_r}(x, y, z) = F^{-1}[F(\widetilde{U_r}) \cdot \tilde{G}]$$

F represents the Fourier transform, and $\tilde{G}$ represents the Fourier transform of the derivative of Green's function.

2.4.3 Digital Holography

Guildenbecher (2014) studied the use of digital in-line holography for measuring particle size of aluminum powder ejected from solid propellant combustion [34]. As the propellant surface burns down, the nano-aluminum particles that were added to the solid propellant melt and form larger particles on the order of micrometers. Models that try to determine the particle sizes of these aluminum agglomerates have a certain amount of uncertainty. Previous investigations in the literature studying these aluminum agglomerations have used many other optical diagnostics such as schlieren, shadowgraphy, videography, line of sight laser diffraction, and point-wise phase Doppler anemometry. Using imaging diagnostics is actually more difficult, though, because each experiment usually can only have one focal plane. To get enough frames with particles that are in-focus requires multiple experiments with varying focal planes. Holography, on the other hand, has the ability to refocus each image after the experiment, allowing one experiment to contain enough data on in-focus particles. In this paper, Guildenbecher et. al. demonstrates the ability to capture a large number of in-focus particles with holography in a single experiment, and classify these particles based on diameter [34].

Guildenbecher (2016) first demonstrated the ability of holography to capture a sufficient number of in-focus particles for data analysis using only one experiment [6]. Most other optical techniques require multiple experiments to be conducted, each with varying focal planes, in order to capture enough in-focus particles. In this paper,

Guildenbecher et al. demonstrate the ability to use digital in-line holography at high speeds to capture velocity vectors of these particles as well as their size. Digital holography experiments have previously been using CCD type sensors to collect data. Although these sensors are great for the resolution of particle diffraction patterns that have high spatial frequency, they are typically low read-out speed sensors. This means that although single experiments are enough to collect particle sizing information, multiple experiments are required in order to string together velocity information. With the advancement of high speed imaging, CMOS camera sensors are now able to capture frames at rates of kHz with around 1-megapixel sized images. In this experiment, a digital in-line holography setup with a collection rate of 20 kHz is proposed for both the tracking and sizing of particles in 3D space. Two types of experiments are conducted, showing the potential of this optical technique. First, water droplets are made from dropping a water droplet onto a thin film of water, and the following drops are studied. Second, aluminum agglomerations from the burning of solid propellants is studied [6].

3. EXPERIMENTAL METHODS

3.1 Experimental Apparatus

3.1.2 Sample Preparation

Firearms are not used in our experiment to determine the concentration of metal particles being ejected during combustion of ammunition. In order to simulate the combustion reaction from firearms in the laboratory, small propellant strands are used, an example of which is shown in Figure 5. As these strands burn down, the resulting flame becomes the zone where the concentration of metal particles is measured. The propellant strands are made in an in-house facility that is a part of the Petersen Research Group. They are composed of ammonium perchlorate (AP), with a hydroxyl-terminated polybutadiene (HTPB) binding material. Additional additives are then added to these strands during manufacturing, depending on the material to be studied. Aluminum nano-powder was the chosen material added to the strands. AP is a necessary material to the strands. Without AP, the binding material burns in a non-energetic fashion. The added metal powder would not react in a fashion that would cause the particles to eject into the surrounding air. The propellant strands are hand-mixed and are created in 20-gram batches. A digital scale is used to measure each component to within 0.01 grams before they are added to the mixture, and the final mass percentages have an uncertainty of ±20%. The metal powder was first mixed with HTPB in order to completely coat the metal particles. Then the AP was added to the mixture, and lastly an IPDI curative was added. After all components are added together, they are mixed according to a process that has been tested to provide repeatable results. This process produces the same results recorded in prior works that

used mechanical mixers instead [35, 36]. All mixing is done below a Labconco fume hood to minimize the possibility of contact with a harmful substance. Air pockets within the propellant mixture is a concern and is mitigated by vacuuming the final mixture. The mixture is the heated to 65°C to lower the viscosity. The uncured propellant mixture is then drawn into Teflon tubes of diameters and lengths approximately 4.76 mm and 30 mm, respectively.

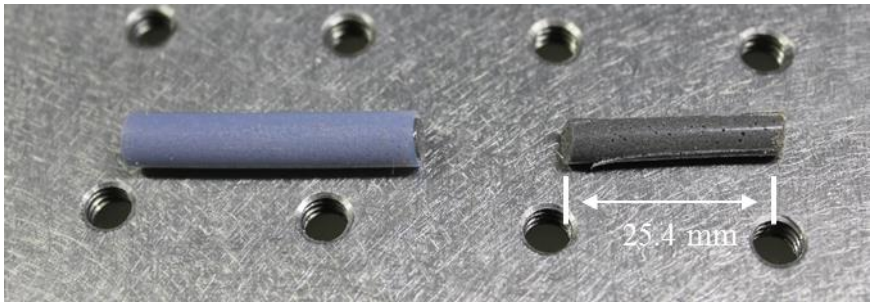

Figure 5. Propellant samples used in present experiments. These samples provide an environment to mimic the combustion of ammunition explosive materials from a weapon.

Once cured, the Teflon tubing was cut away to remove the propellant strands. A burning platform was made of shop-metal to allow for consistent placement of propellant strands and is shown in Figure 6. The strands were ignited with a hand-held torch.

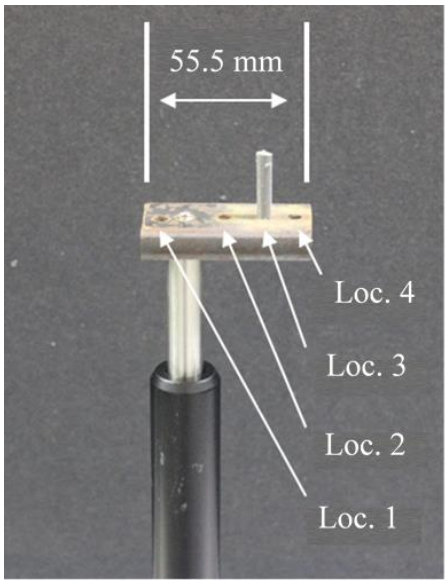

Figure 6. Propellant strand holder. Locations 1-4 are different positions the propellant strand can be placed in.

3.1.2 LIBS Apparatus

Figure 7 displays the optical setup that specifically deals with LIBS. A Continuum Powerlite Nd: YAG laser is used to create the laser spark for LIBS. This laser system can produce two different wavelengths, 532 nm and 1064 nm, each operating at a 10-Hz pulse rate. For the purposes of this thesis, the 1064 nm wavelength was chosen for the LIBS experiments. This is because the desired wavelength under study for aluminum is 396 nm. If the 532 nm wavelength was used, the intensity of light from the laser beam could be far greater than the aluminum LIBS signals detected, making it difficult to discern the aluminum signal. Using a half-wave plate and a polarizer, the power of the laser pulses can be tuned to the specific power desired. This is in contrast to changing the power of the laser pulses by changing the operating voltage of the laser. It is desired to run the laser at

a high enough power such that the laser energy remains as constant as possible between laser pulses. While the laser might be outputting a 1064 nm beam at around 250 mJ/pulse, the half-wave plate and polarizer can be adjusted such that each pulse is only around 200 mJ/pulse at the LIBS detection site. A collimating lens is then placed about 4 inches away from the LIBS plasma site. The light collected is routed through a fiber optic and given to a Princeton Instruments IsoPlane 160 Spectrometer. The IsoPlane 160 is a compact spectrometer that offers the resolution of 1/3 meter spectrometer. Using a 300 g/mm grating with a 300 nm blaze angle, the collected light is diffracted to the constituent wavelengths. A Princeton Instruments PI-Max 4 ICCD camera is used to record the acquired spectra. The camera has an imaging array is 1024 pixels by 1024 pixels, with a pixel size of 13 x 13 µm. The detection limits for this camera are from 200 to 900 nm.

Figures 8-10 display pictures of the optical setup ready for an experiment. Figure 8 gives an overall view of the experimental setup. It is possible to see in this figure that the DIH specific optics are on their own platform, a small 18 in. x 18 in. platform that can be moved to any location while keeping the DIH optics aligned to each other. Figure 9 gives a close-up view of the propellant strand holder, and the imaging camera for DIH as well as the collimating lens for LIBS. Figure 10 displays a close-up view of a propellant strand in the strand holder, with respect to the imaging lens for the DIH setup.

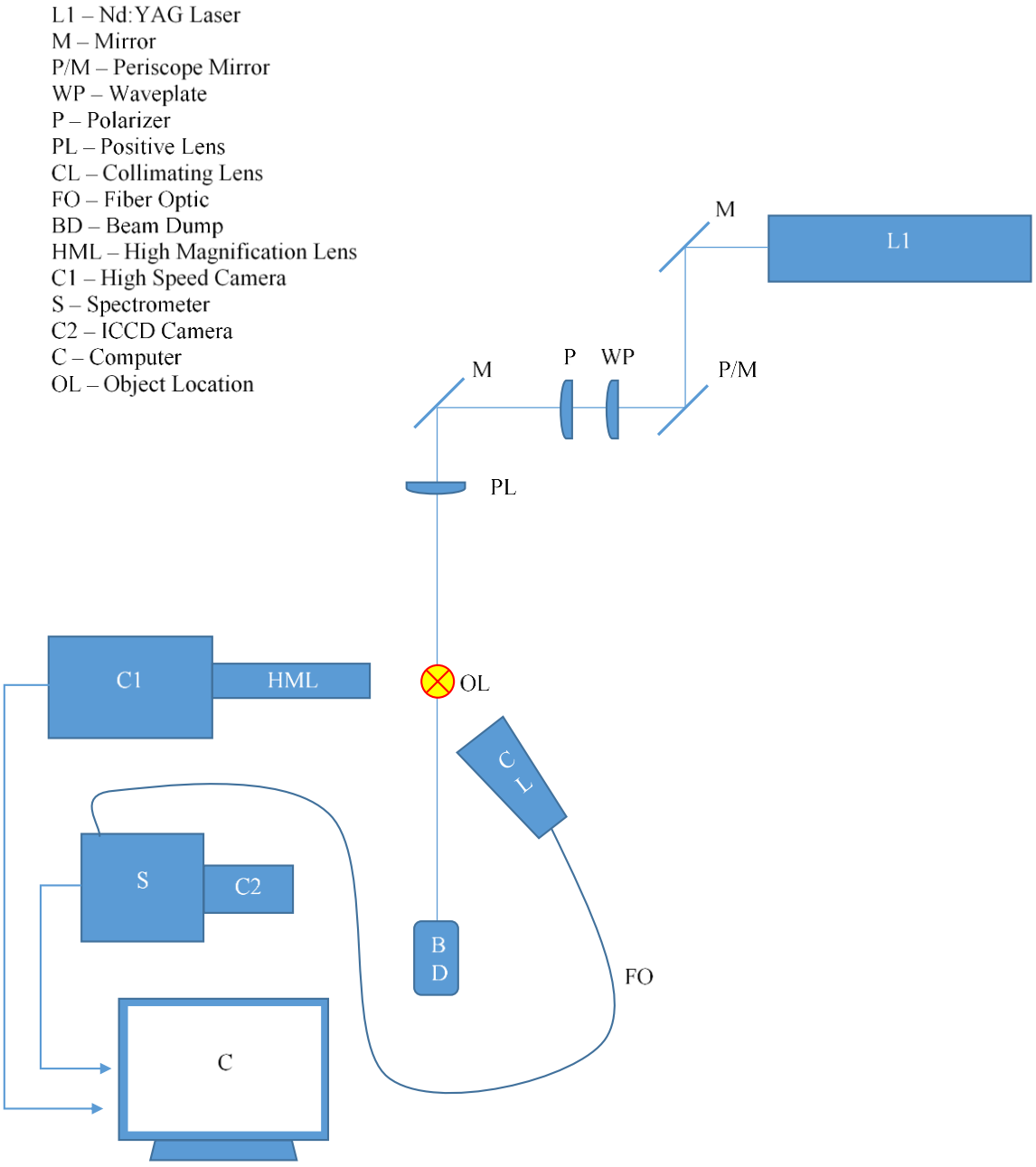

Figure 7. LIBS optical setup used for this thesis research.

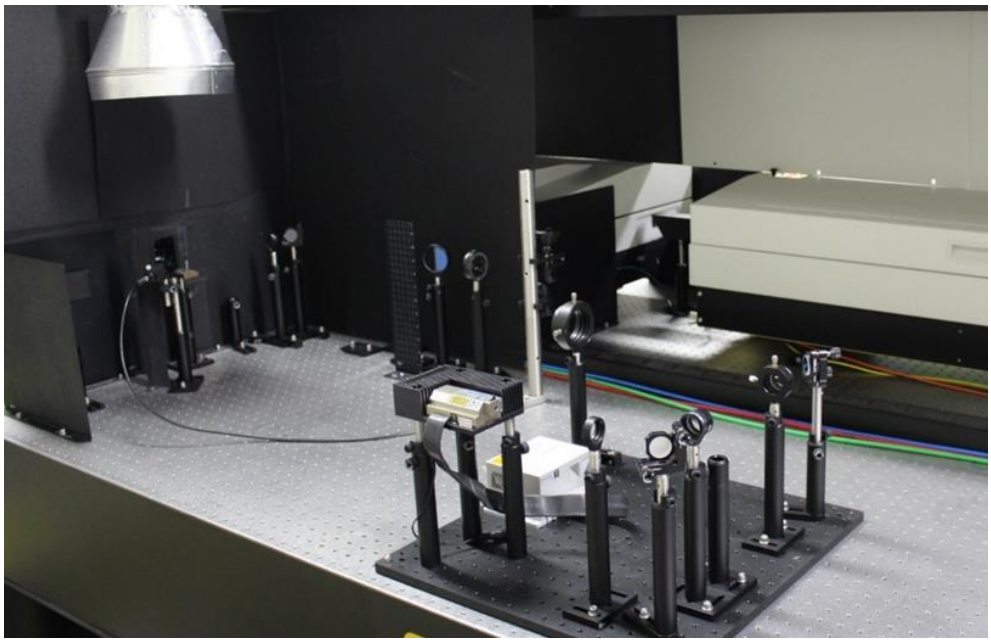

Figure 8. Setup showing LIBS and DIH optical paths.

Figure 9. Close-up of propellant strand holder, DIH lens placed behind a protective window, and collimating lens behind protective window.

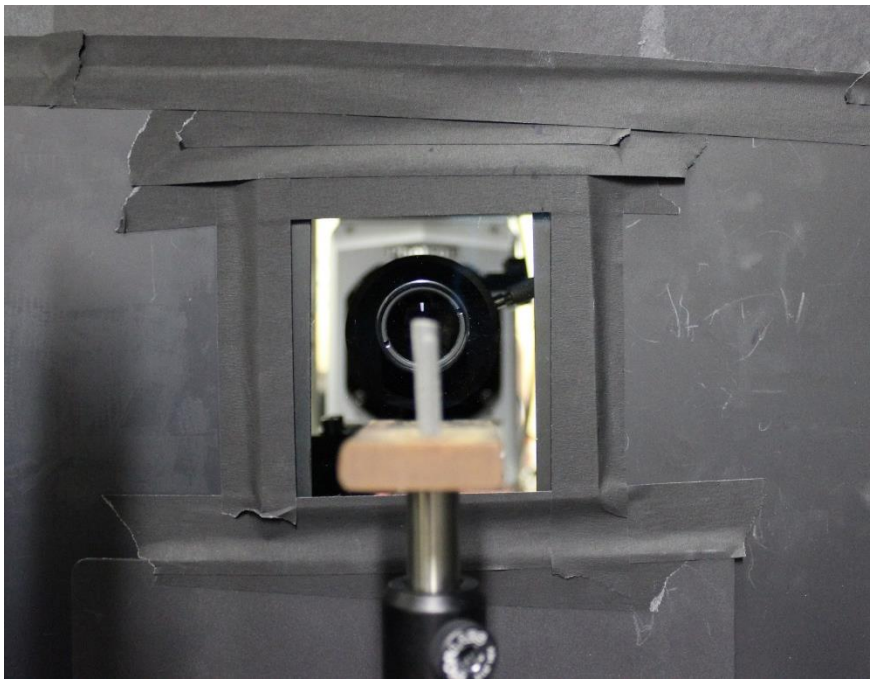

Figure 10. Close-up view of propellant strand in the strand holder, and the DIH lens placed behind a protective window.

3.1.3 Digital In-line Holography (DIH) Apparatus

Figure 12 displays the DIH optical setup and how it is situated in reference to the LIBS setup. For DIH, a continuous laser beam is needed, instead of a pulsed laser beam. A small Oxxius diode laser that operated at 532 nm was used. This beam needs to be expanded before it can be used as a holography beam. In the case of digital in-line holography, the object beam and the reference beam are on the same axis. Thus, several diverging lenses are placed in the optical path to expand the beam to 2 inches in diameter. A positive lens is then placed in the optical path and placed in such a way as to produce a collimated beam with the 2-inch diameter. This expanded beam then illuminates both the particles to be imaged, and the imaging camera. Before the beam illuminates the camera,

it goes through a neutral density filter to cut down the intensity and prevent the camera from saturating. The camera used for these experiments is a Photron SA-Z Fastcam. It has the ability to image up to 2 million frames per second; however, to achieve higher frame rates, the camera bins the CMOS chip to use less pixels. For the purposes of these experiments, the camera is run at 20,000 frames per second, with an exposure setting of 40 μs. Attached to the Photron SA-Z is a high-magnification video lens and objective. The Infinity K2/DistaMax long distance video microscope paired with a CF-4 objective can achieve a magnification between 4.57 and 6.1 at a working distance between 54 and 64 mm. The magnification of this high speed, high magnification optical setup is demonstrated with Figure 11.

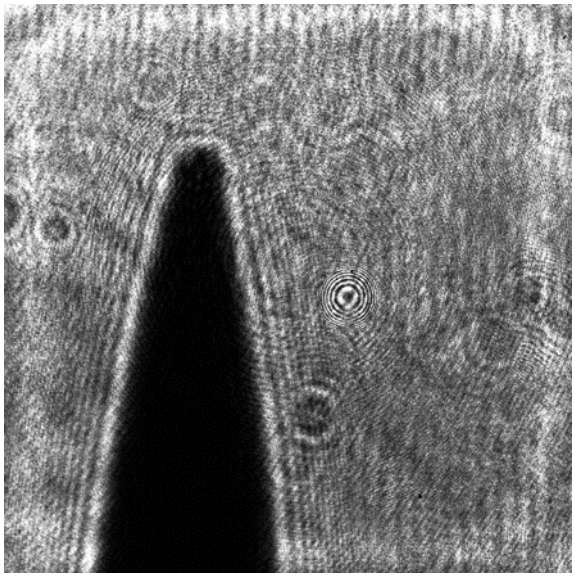

Figure 11. Magnified view of a push-pin tip in the DIH setup.

The tip of a push-pin is shown in this figure. The width of the push pin at the consistent diameter section is 1.1 mm. A quick calculation shows that the magnification of this system is about 6X. Knowing that the sensor which gives the image in Figure 11 is 20.48 mm long, taking a ratio of the pin width to the width of the Figure image gives the pin width on the sensor to be about 6.8 mm. This then gives a magnification on the order of 6X.

Figure 13 shows the DIH optics in the experiment. As mentioned before, these optics are on their own platform so that easy transfer of the entire system can be made without having to realign each of the DIH optics.

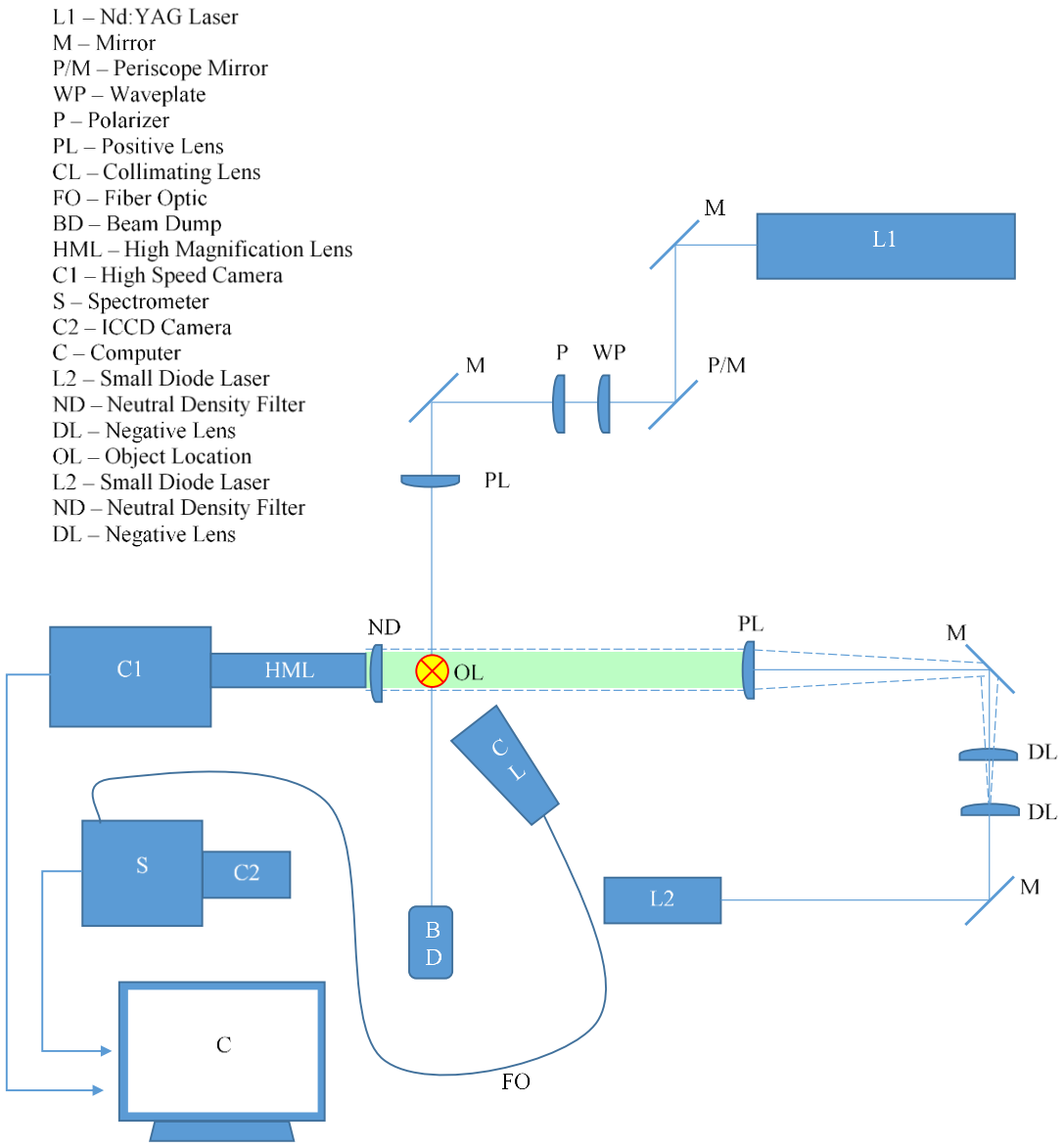

Figure 12. Optical setup now showing the added DIH components.

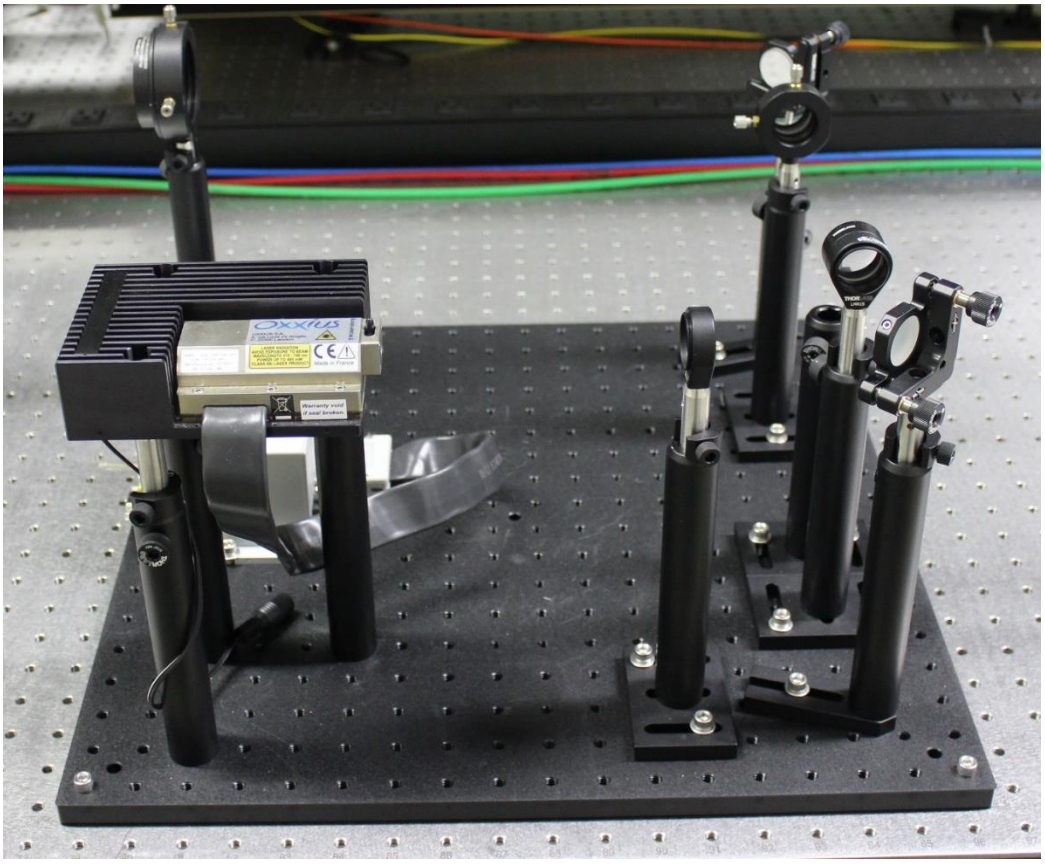

Figure 13. DIH component of the optical train in the laboratory.

3.2 Experimental Procedures

3.2.1 Setting up LIBS System

LIBS is a relatively easy experiment to run. Results can be captured in situ, and the laser spark is non-invasive. The four main parameters revolving around setting up a LIBS experiment include choosing the wavelength of the laser beam, determining the power level, finding an appropriate delay and exposure setting for the camera, and selecting a gain that allows the signals to be detected.

Prior LIBS experiments conducted in propellant flames have been well documented by my colleague and can be found in several resources [5, 29, 30]. It was found that a laser energy of 100 mJ/pulse for a 532 nm beam allowed for a desirable signal-to-noise ratio (SNR) without increasing intensity levels that would lead towards saturation. The main concern with using the 532 nm beam for the experiments in this thesis is that the wavelength under study in LIBS is an aluminum line at 396 nm. While aluminum does have other lines that are detectable, namely at 309 nm and 356 nm; however, during these experiments the 396 nm line produces a much more desirable SNR. When a 532 nm laser beam is used to cause a LIBS spark, the light resulting from the laser beam can sometimes start to saturate the imaging camera, making it hard to distinguish even the 396-aluminum line. Therefore, the 1064 nm laser beam was chosen for these experiments. In order to maintain a similar SNR,

$$E = \frac{h \cdot c}{\lambda}$$

In this equation, h is Planck's constant and is 6.63 x 10^{-34} J·s and c is the speed of light which is 3.00 x 10^{8} m/s. According to this equation, if a wavelength doubles, the energy per pulse would be cut in half. Therefore, if using a 1064 nm laser beam, a laser energy of 200 mJ/pulse would be similar to using a 532 nm laser beam at 100 mJ/pulse.

The camera is triggered to take spectra using the Powerlite laser. Utilizing an output TTL signal that the Powerlite laser outputs from the flash lamps, the spectrometer camera can image at the same rate as the laser pulses, 10 Hz. This signal outputted,

however, is synchronized with the flash lamps, and therefore is not aligned with the LIBS breakdown event. In order to have the camera exposed during the LIBS breakdown, a delay needs to be utilized. By starting with a very wide exposure time and minimal delay, the camera can be exposed during the LIBS event, and spectra can be observed. Then the exposure can be closed a little, and the delay increased some, all while keeping the camera exposed during the LIBS event. Repeating this process can leads to finding the delay to be used to capture LIBS spectra while using a very small exposure time. For this setup, a delay of 256.5 μs was found. An exposure of 300 ns was used for these experiments.

An intensified charge-coupled device (ICCD) camera is able to increase the signal of collected light on the camera chip. This helps to detect spectra when the signals are very weak. However, selecting too large of a gain can cause the camera to become saturated, and possibly burn the camera chip. In these experiments, several gains were compared in order to find one that allowed for ample detection of the aluminum 396 nm line. Gains of 1 and 4 do not allow for the detecting of the 396 nm line, and a gain of 12 produces spectra where the 396 line is clearly distinguishable, however it is close to the saturation limit of the camera, which is 65,000 counts. Therefore, a gain of 8 was chosen for these experiments.

3.2.2 Setting up DIH System

Similar to setting up the LIBS experiments, setting up DIH experiments revolve around a few main parameters. The laser intensity, the placement of the strand in reference to the imaging lens, and calibrating the system are the main issues that need to be addressed.

The small diode laser used for these experiments had no power control. The laser outputted a continuous wavelength of 532 nm light with a power of about 25 mW. However, if the total power of this laser beam illuminated the camera, it would saturate the CMOS chip. Therefore, a neutral density (ND) filter is used to cut down the intensity of light illuminating the camera. In order to choose the best ND filter, several filters were compared. Figure 14 shows the comparison of three different ND filters, with optical density (OD) of 1.5, 2, and 3.

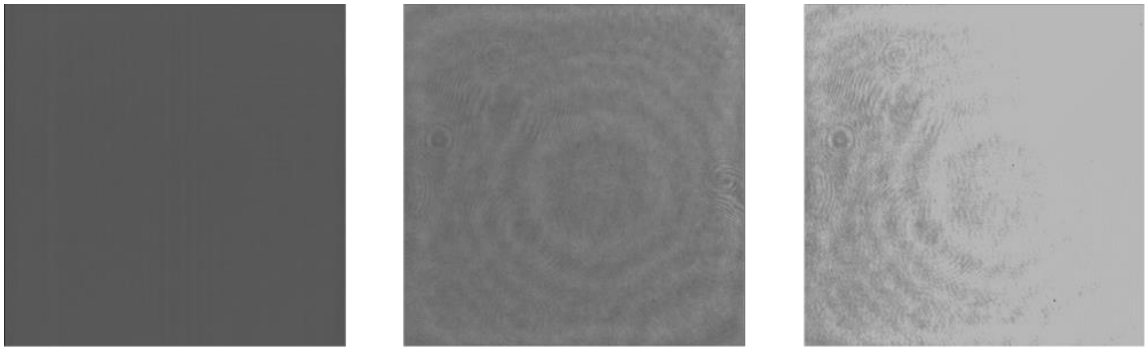

Figure 14. Comparison of ND filters used for DIH. (A) OD = 1.5. (B) OD = 2.0.

From this figure it can be seen that an ND of 2 provides enough illumination on the imaging camera without saturating it. The next parameter to determine is the placement of the propellant strand with reference to the imaging lens. Figure 15 shows the DIH optical setup and illustrates two important parameters here. Length ‘a’ is the distance between the propellant strand, measured at the center, and the imaging lens. Length ‘b’ is the focal length of the imaging camera. In these experiments, the focal length is 55 mm.

Referencing Figure 6, the propellant strand can be placed in one of several different ‘a’ length locations.

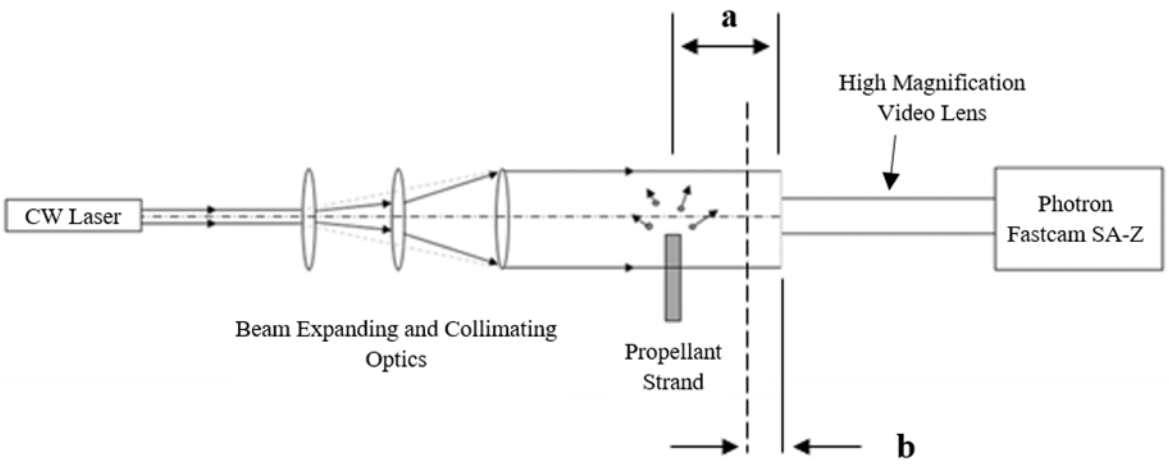

Figure 15. DIH optical schematic. Length ‘a’ refers to the distance between the propellant strand and the imaging lens. Length ‘b’ is the distance between the imaging lens and the focal plane.

A simple experiment using locations 1, 2 and 3 was used to compare data collected at each location in order to determine if one location was better than another. The results are displayed in Figure 16 below.

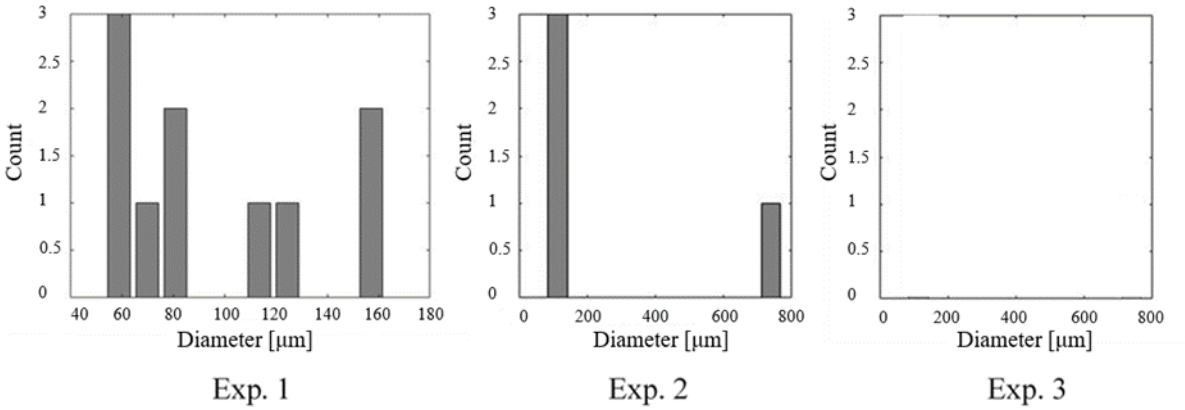

Figure 16. Experiments showing the effect of different propellant strand placement locations.

The diameters in experiment 1 have a range of 60-160 micrometers, with an average of 83 micrometers. The diameters in experiment 2 have a range of 150-750 micrometers, with an average of 282 micrometers. The number of particles captured in experiment 1, however, are significantly greater in number than in experiment 2. Experiment 3 had the propellant sample placed at 0.5 inches, but no particles were captured at this distance.

Before each experiment, the imaging lens is focused to a plane around 2 inches in front of the lens using a 1951 United States Air Force resolution test target, shown in Figure 17. This serves two purposes: to focus the lens on the same plane before each experiment and enable determination of the resolution of the images taken. Figure 18 displays a zoomed-in image of Figure 17, allowing the determination of the smallest distinguishable line pair on the target. The smallest distinguishable pair was taken to be the 6-2 grouping.

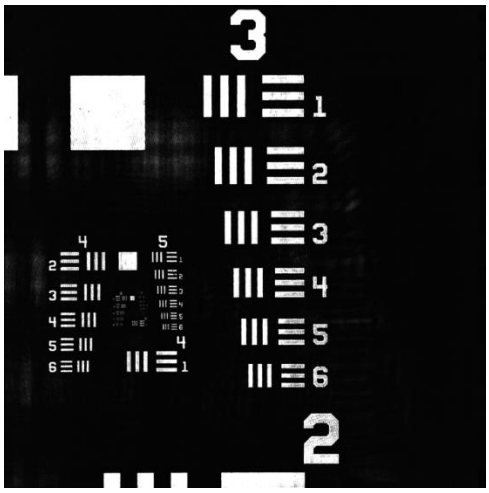

Figure 17. Determining the resolution of the DIH system.

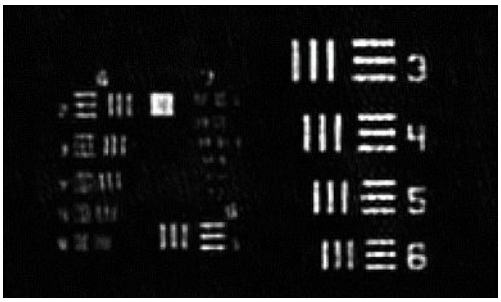

Figure 18. Zoomed view of Figure 20, showing the smallest line pine grouping to be distinguished is the 6-2 group.

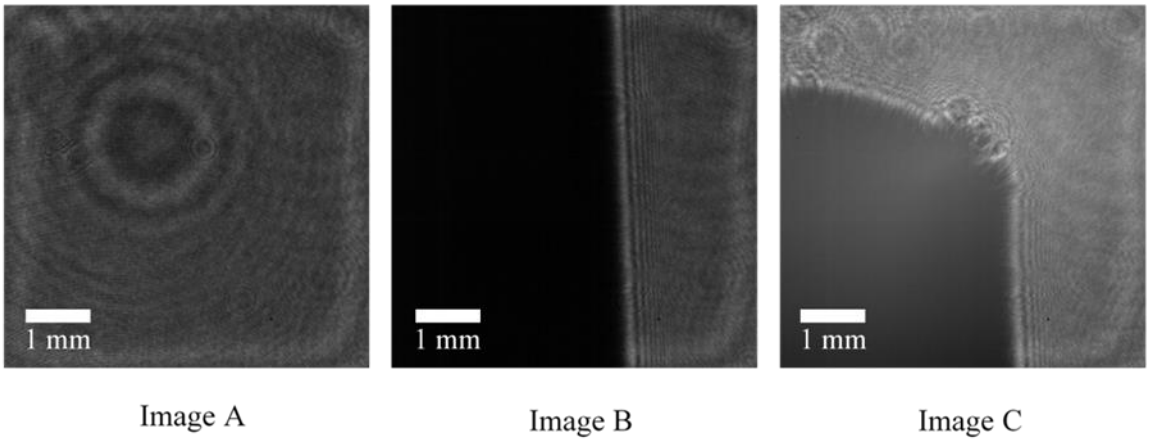

Figure 19. Image A: Field of view of camera before strand is put into place. Image B: Field of view once strand is ready to be ignited. Image C: Field of view while strand is burning. In Image B, the strand extends above and below the field of view by about 1-inch.

Figure 19 shows how the propellant strand is placed height wise. Image A in Figure 19 shows the field of view of the camera. The noticeable haloes in the image are diffraction circles that are most likely due to stray particles either in the air floating, are on optics, or are on the protective glass that sits between the imaging lens and the burning propellant strand. Image B shows a propellant strand that is placed in the strand holder and displays how the strand exceeds above the field of view of the camera. The propellant strands are placed like this for each experiment and are then lit using a hand-held torch. The high-speed camera is triggered to start imaging by the user. Setting up the propellant strands as in Image B is helpful so that once the strand burns down past the field of view of the camera, imaging can be triggered to start taking place.

3.2.3 Analyzing DIH Data

Setting up the Photron SA-Z camera to image at 20,000 frames per second, with an exposure timing of 40 µs per frame, allows for roughly 1 second of data to be collected. Around 21,000 frames are collected, but only certain portions of the total amount are saved, depending on the phenomena observed. Figure 20 shows a sample sequence of frames collected from an experiment.

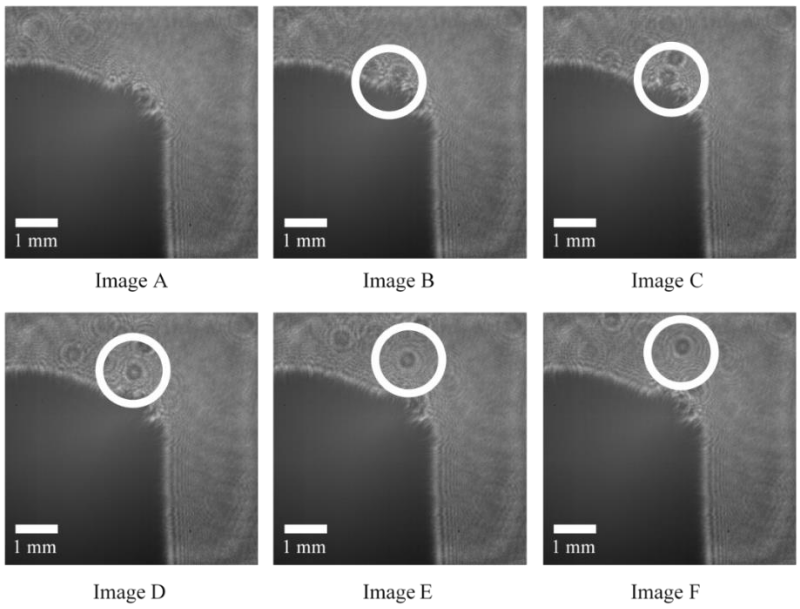

Figure 20. Images A-F are sequential in order. Time between frames is 15 microseconds. The circles are tracking a metal particle that is ejected from the burning strand.

The circles follow a metal particulate that was initially on the strand, and then is ejected into the reacting flame. These are the objects that are under study in these experiments. Classification of the size, spatial location, velocity, and density of these objects will help to understand the particle field that future LIBS signals will study.

The experimental data were analyzed using a series of MATLAB scripts, written by Dr. Daniel Guildenbecher at Sandia National Labs. To give a general overview of this, the scripts start with a single frame and go through 20,000 frames one by one in chronological order. For each frame, the MATLAB scripts numerically refocus the frame, looking for particles in focus. Through this approach, the script is able to identify different particles on that frame, and characterize them by diameter, depth, and x-y location. The script then does this for the next frame, and so on until all frames are analyzed. At the end of this step, a matrix will have been created with all particles captured. The next step is to go through a particle matching algorithm. Objects that are collected are compared from frame to frame to determine whether or not they are the same particle moving through space. If they are, then the object is kept. At the end of this comparison step, the scripts produce a video of the frame moving at a slower speed and will draw a circle around objects that are identified as particles. If the scripts determine that some of the objects it initially captured are not actually particles, it will delete them from the matrix. Dr. Daniel Guildenbecher of Sandia National Laboratories has documented the development of his DIH imaging techniques and analyzation techniques in several papers [6, 33]. The Sandia Particle Holography Processor code (HoloSand) was made available to us through an end-user agreement between Sandia National Laboratories and Texas A&M University. Figure 21 shows the ability to find objects in an image by refocusing the image.

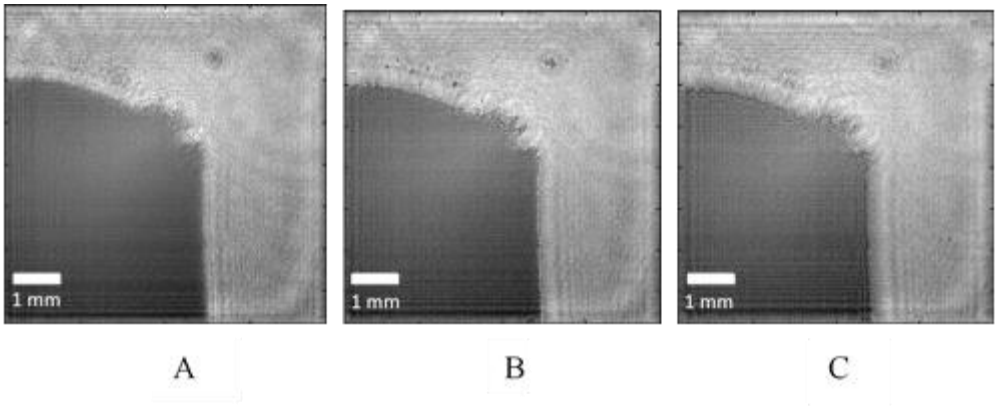

Figure 21. Each of these frames are the same image. MATLAB scripts have been used to numerically re-focus frames B and C. Frame A: z = 78 mm. Frame B: z = 128 mm. Frame C: z = 178 mm.

Each image in Figure 21 is the same frame from an experiment. The sample propellant strand is the large dark object in the bottom left of each image. The metalized particulates being ejected from the strand are the tiny objects just above the strand in each image. In image A of Figure 21, none of the metalized particulates are in focus. Instead, you can see small rings in various parts of the image. These small rings are interference patterns emerging around the particles. As the depth of focus is changed, these small particulates can come into focus. Image B shows more particles directly in focus, and then image C shows particles becoming out of focusing again.

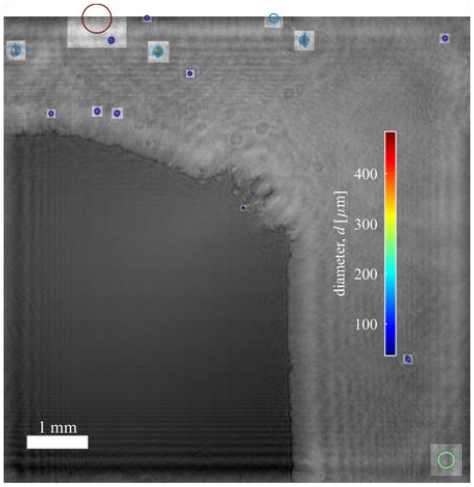

Figure 22. Frame showing the results of the particle recognition algorithm.

Figure 22 shows the ability of the code to discover particles within the flow field. In this case, the image is showing the diameter of different particles that are captured by using a color bar. Knowing where these particles are in three-dimensional space, and then where they are in sequential frames at a given frame rate helps to them back out velocity information.

Figure 23 shows an example of the MATLAB code to detect moving particles. In this example, a 16% aluminum strand is used, and is placed at 3.3 inches from the imaging lens. In this figure, each circular dot is a particle, and some particles are actually the same particle just at different points in time. The analyzation techniques that the code utilizes determines which of these circular dots are the same particle and draws a line through them. This figure shows that some of the particles are tracked, by many are not. Changing user inputs into the code allow for a better analysis of the data, or in some cases a worse

analysis like in the figure below. Correctly measuring the resolution of the DIH system is one parameter that needs to be verified for use in the analysis.

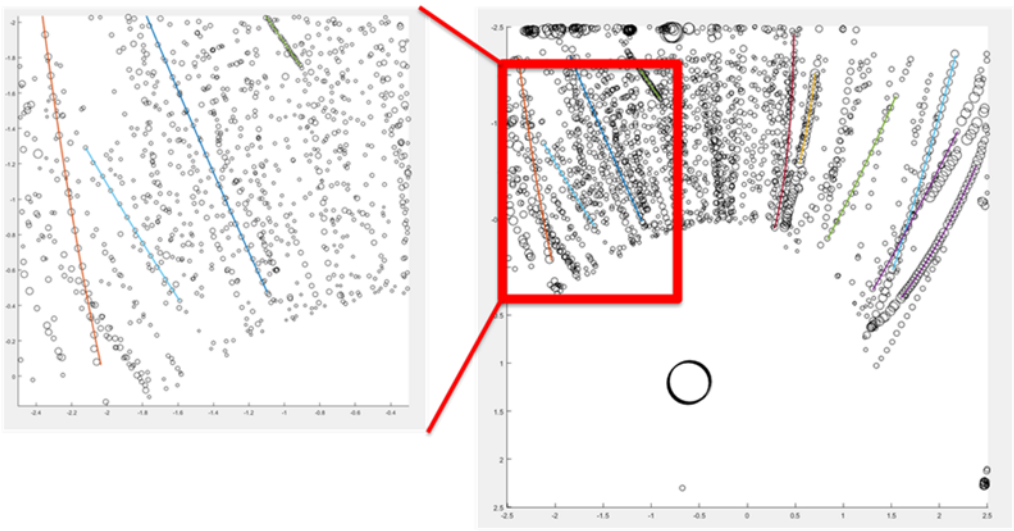

Figure 23. MATLAB showing path lines for all particles recognized during the 16% aluminum sample placed at 3.3 inches. Zoomed in portion shows how particle tracking algorithm correctly identifies only a select few particles as actually being particles.

4. RESULTS AND DISCUSSION

4.1 LIBS Only Results

Collecting LIBS spectra of metal particles within a combustion flame does not produce consistent results in a manner similar to LIBS on a solid plate. In this study, the aluminum line at 396 nm was the source that signaled whether aluminum was detected or not. In a solid propellant with metal powder added, as combustion of the strand occurs, the metal particles are ejected into the atmosphere. The schematic in Figure 24 displays how a LIBS spark location relates to the propellant strand.

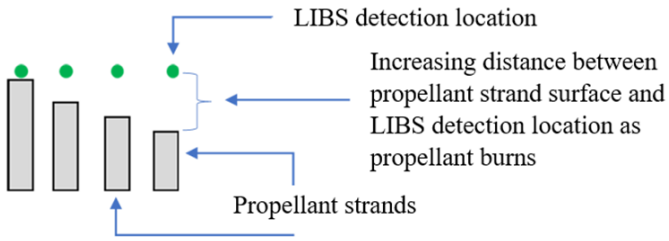

Figure 24. Schematic showing LIBS detection location becoming further away from propellant surface as the propellant burns.

As the propellant strand burns down, the LIBS spark remains in a constant location. Although a future study should characterize the effect of maintaining the LIBS spark at a constant distance from the propellant surface, in these experiments the metal particles were observed through DIH to still be present in the vicinity of the LIBS spark. It should be noted, though, that although the LIBS spark and metal particles are both within

the field of view of the DIH camera, the metal particles are not everywhere present within the field of view. There is empty space, open atmosphere, all around the metal particles. The main consequence of this is that the LIBS spark may not always detect aluminum particles. Sometimes, as in plot A of Figure 25, the LIBS spark may be detecting elements from the atmosphere. In plots B and C of the same figure, aluminum is detected, but at different intensities. This is most likely due to the amount of aluminum particles, or the size of the particle, that was struck by the LIBS spark.

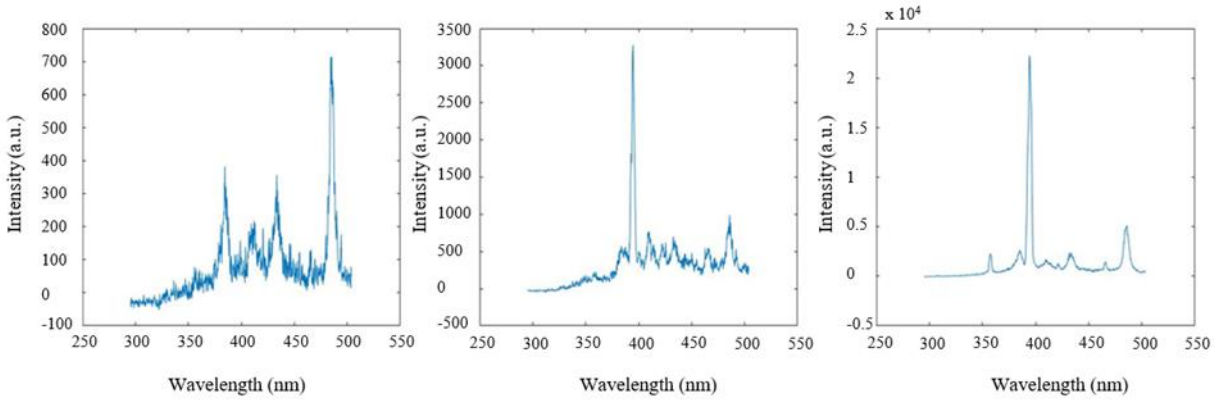

Figure 25. LIBS signals in an experiment searching for aluminum particles sometimes hit aluminum particles, and sometimes do not. (A) LIBS spark did not detect aluminum. (B) LIBS spark detected aluminum, though the intensity detected was low. (C) LIBS spark detected aluminum at a much higher intensity.

This phenomenon of varying aluminum signal detection shapes how data is collected and analyzed. In the experiments conducted with LIBS as the only diagnostic, propellant strands were cut to lengths of 26 mm, and allowed to burn to completion. Each burn lasted roughly 15 seconds, allowing for 150 laser shots that had a chance to create plasma while the combustion flame was present. Figures 26-28 display all the collected

laser shots detecting aluminum at 396 nm for three different samples – 5%, 10%, and 16% aluminum by weight propellant strands.

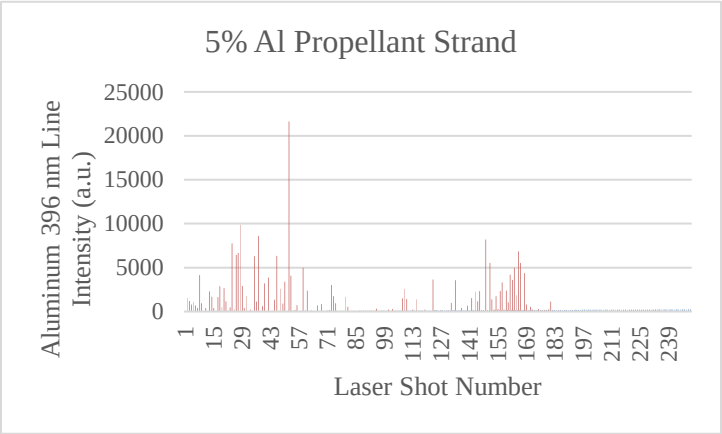

Figure 26. 5% aluminum propellant strand LIBS experiment.

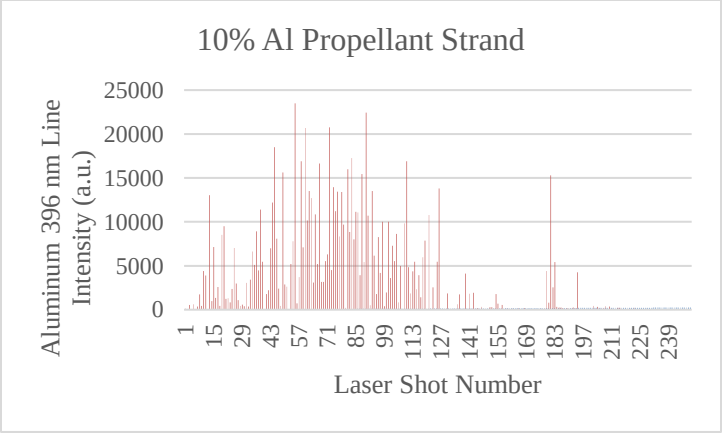

Figure 27. 10% aluminum propellant strand LIBS experiment.

It is evident that as the percentage of aluminum powder within the propellant strand decreases, the number of the laser shots that detect aluminum decreases. Roughly 76% of the laser shots detected aluminum in the 16% Aluminum experiment, about 64% of the shots detected aluminum in the 10% aluminum experiment, and about 46% of the laser shots detected aluminum in the 5% aluminum experiment.

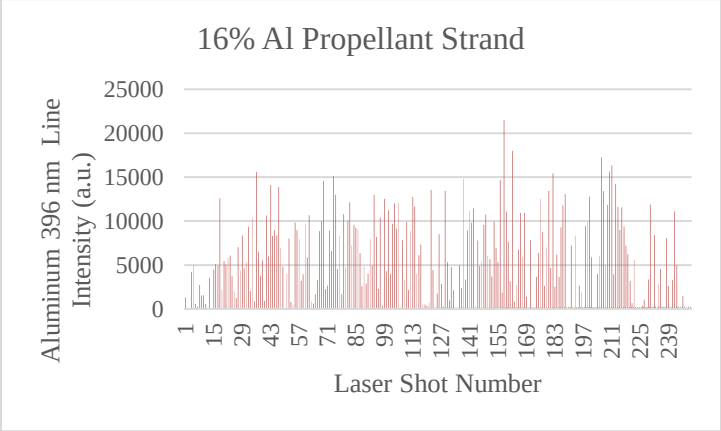

Figure 28. 16% aluminum propellant strand LIBS experiment.

4.2 DIH and LIBS Results

The DIH setup has a field of view of about 13 μm x 13 μm. The LIBS spark has to be placed within the area so that the DIH imaging system can visually see the LIBS spark. The preliminary experiments involved using the pin-head of a push-pin to align the LIBS spark to the DIH system. The push-pin was placed at the focal point of the camera so that the tip was clearly in focus. Then, with the DIH lens covered so as to not risk saturating the system, the LIBS spark was placed to ablate the tip of the push-pin. In this way the

LIBS spark was placed to be in the field of view of the camera. Figure 29 displays the DIH camera imaging a LIBS breakdown plasma in atmosphere next to the push-pin tip. The illumination of the plasma is not enough to visualize the push-pin. Note that although this is imaging with the DIH camera, this is not a DIH experiment. The DIH laser is not illuminating the object field. Rather, that is just the illumination from the LIBS plasma. Once the LIBS plasma was observed to be at the focal plane of the DIH imaging lens, the LIBS spark was shifted back to the plane of the propellant strand, again using the push-pin as a guide.

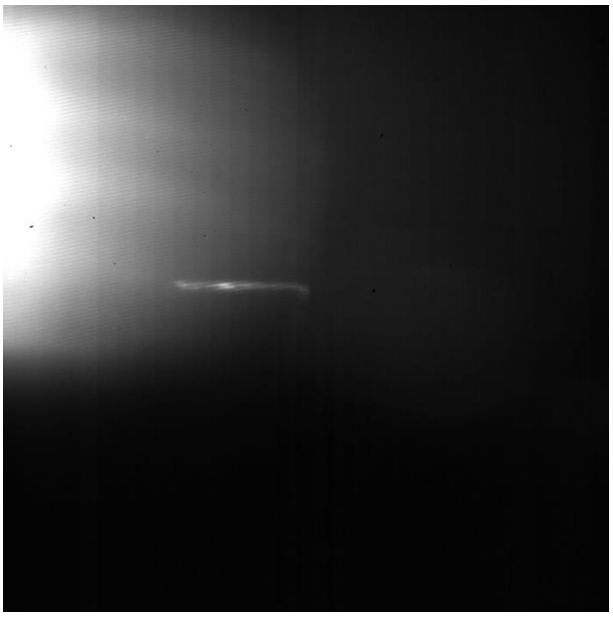

Figure 29. DIH camera imaging a LIBS spark. The DIH laser is not on.

Figure 30 demonstrates the LIBS spark being imaged in a DIH experiment. Each image in Figure 30 is a subsequent frame in the experiment, with 50 μs separating each

frame. Frame number 1 is in the top left-hand corner, and frames proceed sequentially to the right and then to the next row starting on the left.

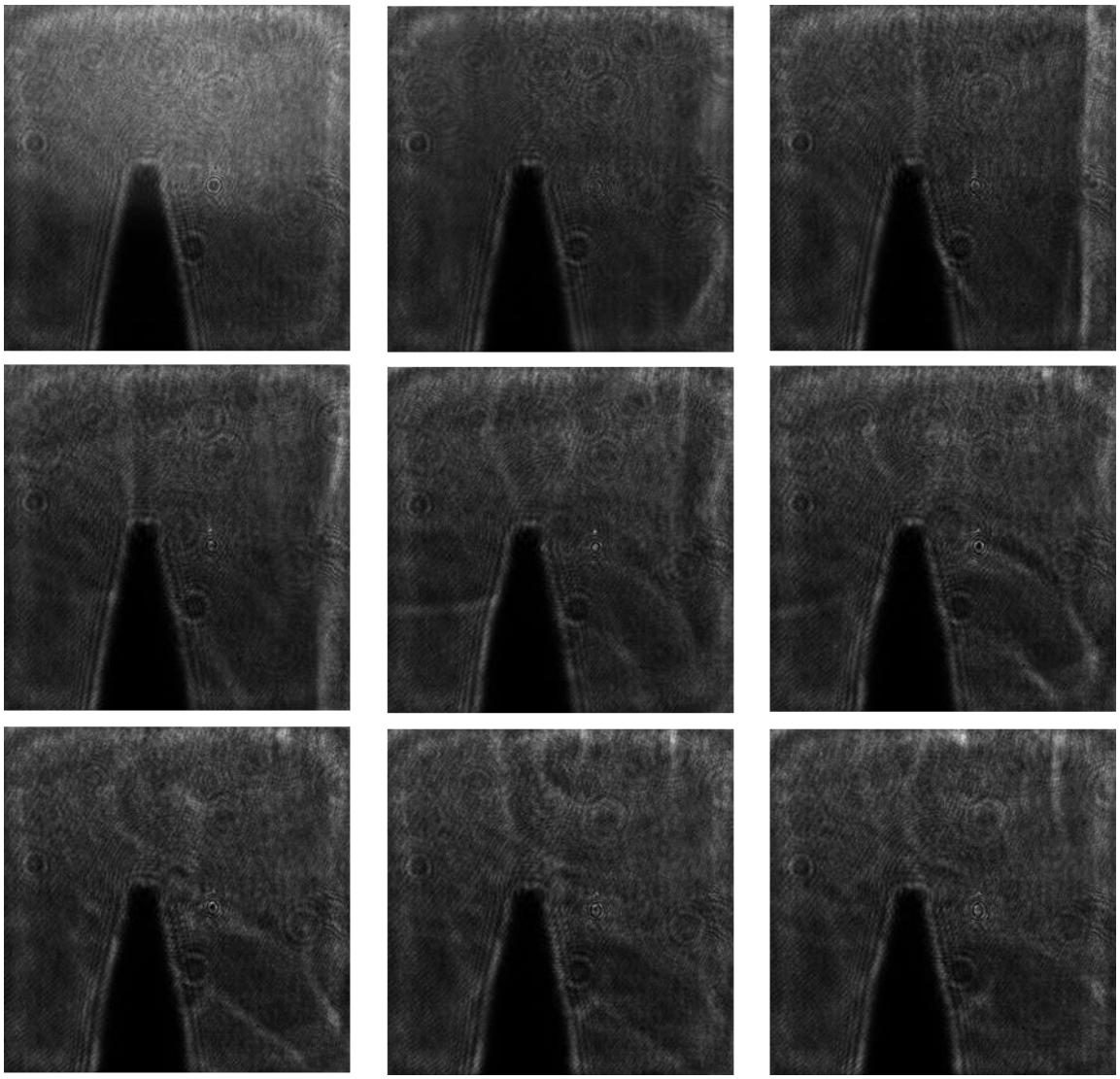

Figure 30. DIH capturing a LIBS spark ablating a push-pin. The DIH laser is on and camera focused on a plane 84-mm away from the laser line.

In frame 1, the top half of the frame has more illumination than the bottom half. This is caused by the LIBS plasma. In subsequent frames shock waves from the plasma can be visualized. Figure 31 shows a timing diagram displaying how DIH collects data compared with LIBS.

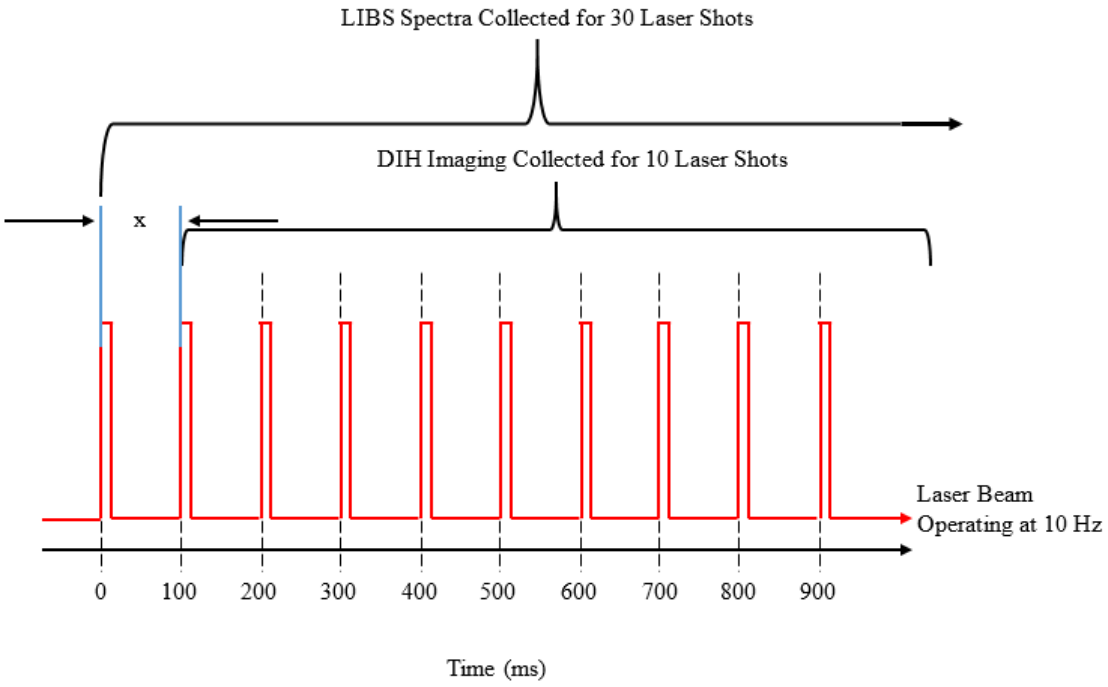

Figure 31. Diagram showing how LIBS and DIH information are collected in reference to the laser pulse. The delay 'x' is user induced, and unknown.

The laser beam is shown to be pulsing at a rate of 10 Hz. Each pulse lasts about 10 ns, which is not to scale on this plot, but each pulse comes every 100 ms. Both the LIBS imaging system and the DIH camera are triggered to start taking data by the user with a mouse click; however, each system is on a different laptop. Triggering the experiments in

this way places an unknown delay, x, between the collection of data between LIBS and DIH and is shown in Figure 31. The LIBS system is then triggered to take 30 different spectra, one per laser shot, for 30 laser shots. The DIH system on the other hand is only phase locked with the laser pulse. This means that the first laser shot after the user triggers the DIH camera to start imaging causes the camera to start taking data. At this point, however, the camera takes images at 20,000 frames per second, irrespective of the laser pulse. It was observed that after several laser shots, although the DIH system was phase locked with the laser pulse, the DIH images started to drift away from the laser pulse. It is uncertain whether this is caused by the laser pulse, the DIH camera, or both.

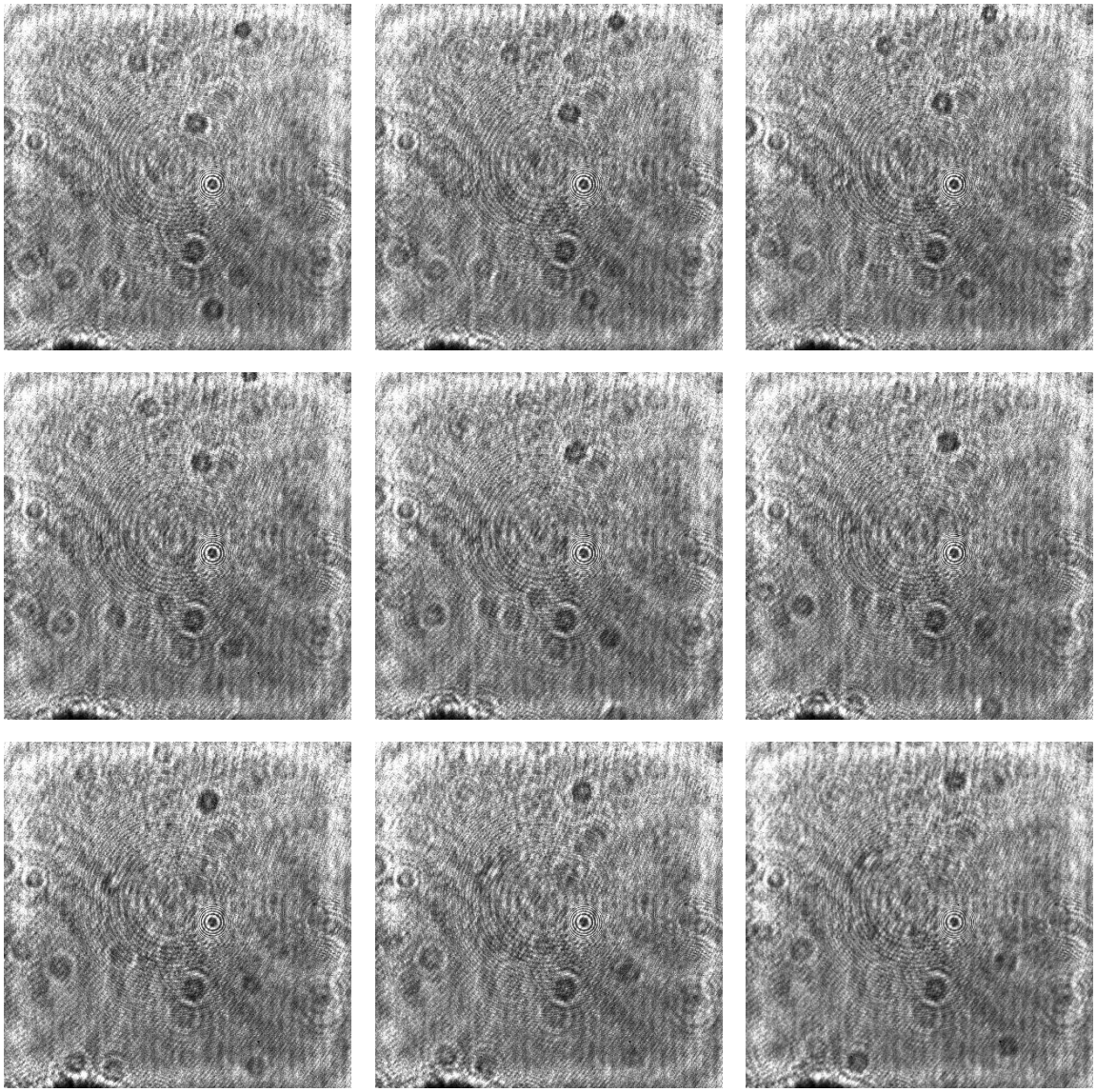

Figure 32. DIH and LIBS experiment while burning a 16% Al propellant strand.

Figure 32 displays a portion of the data collected from the burning of a 16% aluminum propellant sample. In this experiment, both LIBS and DIH were conducted. The LIBS spark occurs once every 100 ms, and therefore can be imaged by the DIH camera once every 2,000 frames. The frames in Figure 32 surround the first LIBS plasma observed

by the DIH camera. In these frames, however, the DIH plasma is unnoticeable. The frames selected are suspected of containing the LIBS plasma because experiments both before and after this experiment without the DIH laser running or the propellant burning show the plasma being imaged as in Figure 30. It is unknown currently as to why the plasma is not observable while the propellant strand is burning. One reason may be due to the breakdown threshold in atmospheric air compared to the propellant flame. Initial experiments were conducted with a LIBS pulse energy of 200 mJ, and then increased to around 230 mJ per pulse to determine if the plasma could be observed. The plasma still could not be seen with this higher laser pulse energy. Higher pulse energies are a concern, though, because although this higher energy causes an adequate plasma that can be seen within the combustion flame, once the flame extinguishes the plasma occurs in atmosphere at a much higher intensity which could saturate the imaging camera. Although an ND filter that blocks out more light from entering the DIH camera could be used, this would adversely affect the DIH experiments, making metal particles harder to distinguish.

The DIH data collected from this experiment is shown in Figures 33-38. Particles are observed to be on the order of several hundred micrometers. This is in good comparison with similar experiments conducted in the literature [6, 33].

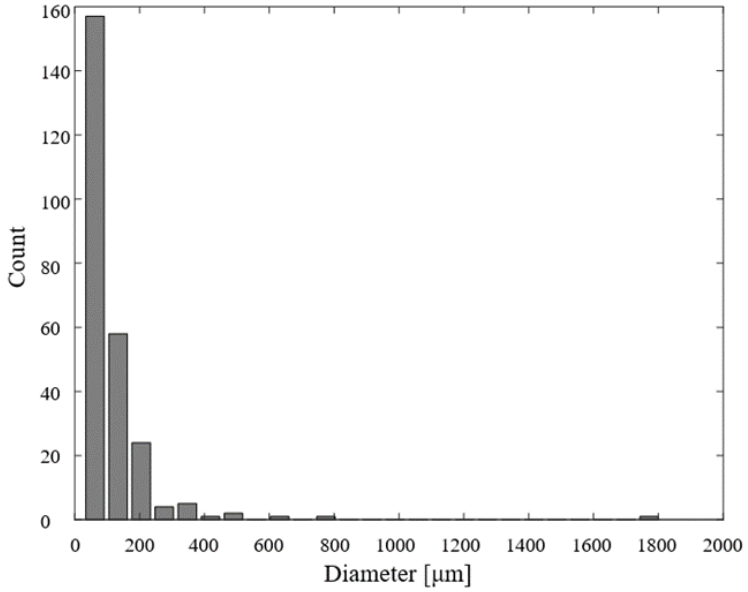

Figure 33. Particle diameter histogram from 16% aluminum propellant strand burn.

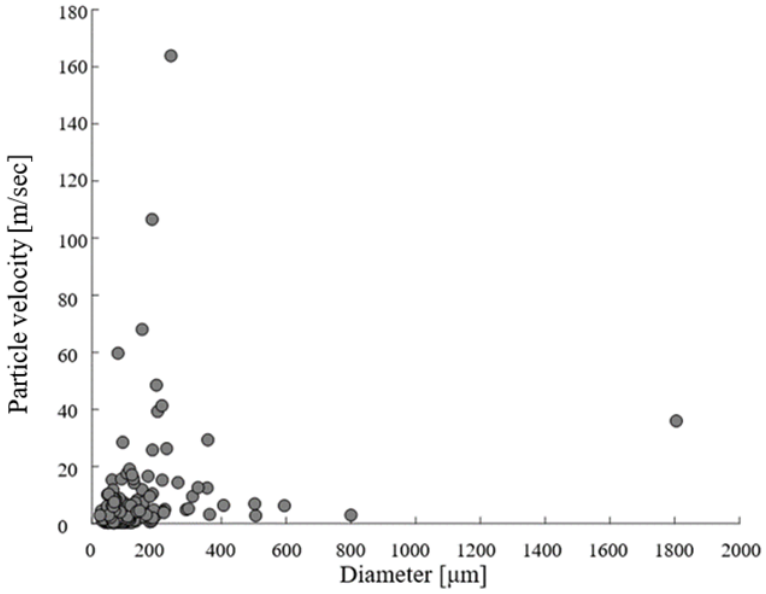

Figure 34. Total particle velocity compared to particle size.

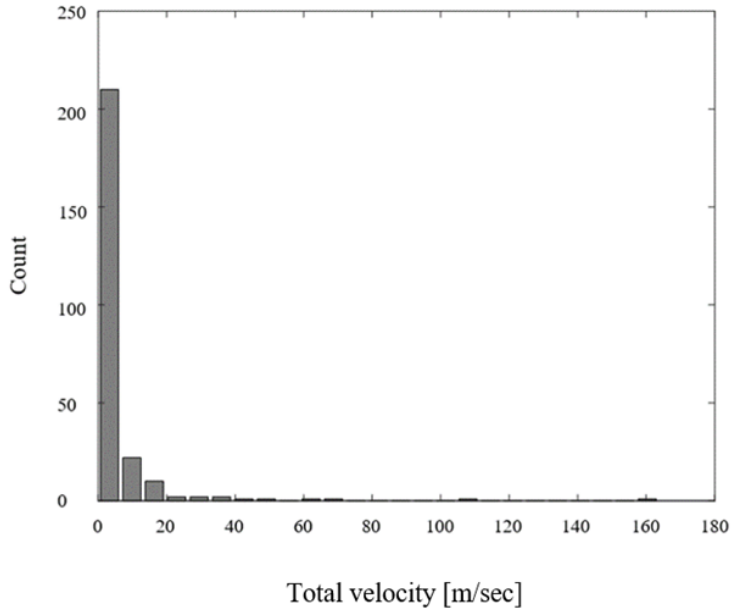

Figure 35. Total velocity histogram.

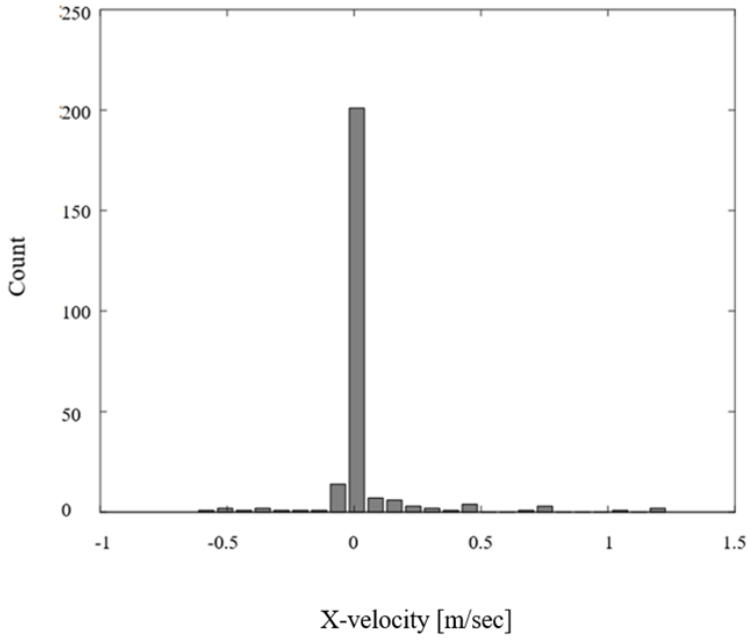

Figure 36. X-velocity histogram.

Figure 34 displays a comparison between the total velocity of a particle and its diameter. Most of the particles that were captured are 200 μm or less, which is shown in Figure 33, and are moving at less than 10 m/s, shown in Figure 35. Figures 36-38 display the velocity components of the particles that were captured. Looking at these paints a picture of how these particles moved across the field of view of the imaging camera. Figure 35 gives the total velocity of the particles, with most particles displaying speeds of less than 10 m/s. In Figure 36, most of the particles moved at some speed between -4 and 4 cm/s in the x-directions. Most of these particles weren't moving completely to the left or right directions in the field of view, but rather moving more straight up or down in the field of view.

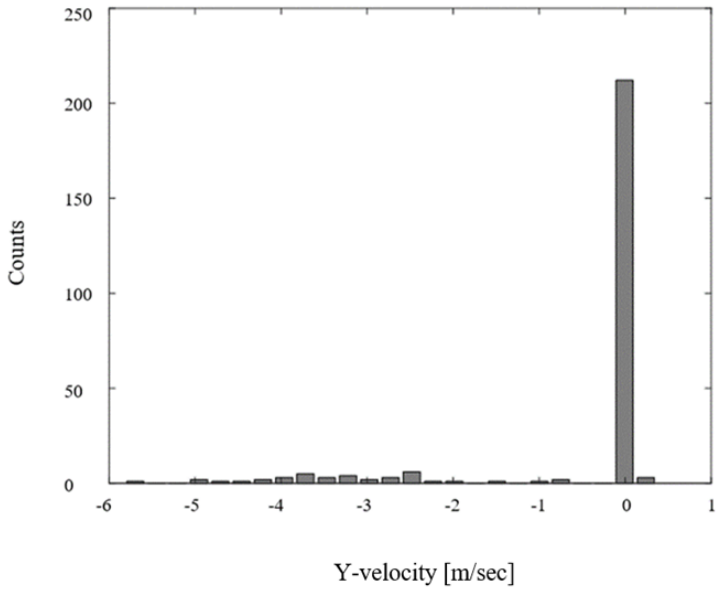

Figure 37. Y-velocity histogram.

Figure 37 displays the y component of these particles. Most of the particles were again moving between -4 and 4 cm/s. There were other trace particles captured having velocities up to -4 m/s. These were most likely particles that were falling back down through the field of view. Figure 38 shows the z component of the velocity. Most of the particles had a positive z velocity between 0 and 4 m/s, with a symmetrical number of particles both going in the positive and negative depth directions.

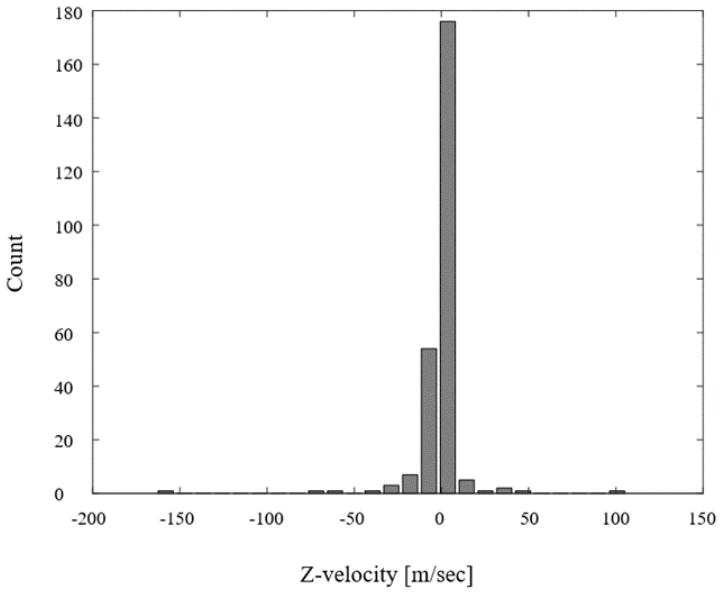

Figure 38. Z-velocity histogram.

5. CONCLUSIONS

5.1 Conclusions

The work presented in this thesis was focused on two aspects of heterogeneous combustion in particle laden flow fields such as burning propellants. The two areas of focus are the chemical signature and physical properties such as position and velocity of reacting solid particles. Ammunition propellant contain organic compounds that provide the necessary conditions for an explosive nature. Metal particulates can then be added to change the combustion characteristics, tailoring the combustion for specific requirements in terms of blast pressure or heat of reaction. The initial research project by my colleague was geared towards studying the use of LIBS for conducting concentration measurements of metal particles within a combustion flame, which is modeled using propellant strands. These initial experiments with LIBS showed promise, but in order to make measurement capture more likely, an understanding of the particle flow field within the combustion flame was needed. This led to the path for the current research work. Aluminum was the only metal particles studied, and different concentrations of aluminum were studied using the LIBS experimental apparatus. In the initial LIBS-only experiments, a good correlation was found between the ability to detect aluminum particles and the concentration of aluminum by weight, within the propellant strands. When combining DIH with LIBS, data collection becomes more complicated. Therefore, only the 16% aluminum case was studied in detail. It was found that the LIBS plasma could not be visualized at the same time as conducting DIH when the propellant strand was burning. Particles were still detected, with diameters averaging between 100–200 μm and total velocities averaging

less than 10 m/s. The z-velocity component, movement in depth, was the component that contained most of this velocity. The x and y velocity components combined to depict that particles moved relatively straight up and down in the field of view of the camera.

5.2 Recommendations for Future Work

Conducting simultaneous DIH and LIBS experiments proved promising but needs further improvements for complete particle flow filed analysis. Moving forward, there are several items that might be helpful in pursuing this goal. First, increasing the power of the LIBS laser might help to see the laser spark while the propellant strand is burning. The difficulty in this is that the breakdown threshold in air is substantially less than within the propellant flame. As the laser energy is increased, it becomes dangerous because once the propellant flame burns out, the resulting breakdown event in air could saturate the high-speed camera. However, if precautions can be taken to prevent this saturation, increasing the laser power might prove very helpful.

Second, these experiments conducted LIBS and DIH as simultaneous as possible without using delay generators. The user had to trigger each experiment to start separately, but as close together as possible. Future experiments should utilize delay box generators that delivers one trigger signal to each the LIBS and DIH experiments simultaneously.

Lastly, conducting high-speed DIH with 10-Hz LIBS experiments can be improved by conducting both laser diagnostic techniques at high speed. Using a higher repetition rate laser, such as a pulse-burst laser, can deliver the amount of laser pulses necessary to conduct LIBS at a kHz repetition rate, similar to the rate at which DIH was conducted in this thesis.

REFERENCES

[1] A. Rezaei, et al., "Approach for Determination of Detonation Performance and Aluminum Percentage of Aluminized-Based Explosives by Laser-Induced Breakdown Spectroscopy," *Appl. Optics,* Vol. 55 (12), 3233-3240 (2016).

[2] J. Wilson, "Space Shuttle: Solid Rocket Boosters," https://www.nasa.gov/returntoflight/system/system_SRB.html.

[3] C. Chang, "The Immune Effects of Naturally Occurring and Synthetic Nanoparticles." *J. Autoimmun.*, Vol. 34 (3), J234-J246 (2010).

[4] A. Miziolek, V. Palleschi, and I. Schechter, *Laser-Induced Breakdown Spectroscopy (LIBS): Fundamentals and Applications* (Cambridge University, 2006).

[5] M. O'Neil, et al., "Laser-induced-breakdown-spectroscopy-based detection of metal particles released into the air during combustion of solid propellants," *Appl. Optics,* Vol. 57 (8), 1910-1917 (2018).

[6] D. Guildenbecher, M. Cooper, and P. Sojka, "High-Speed (20 KHz) Digital In-Line Holography for Transient Particle Tracking and Sizing in Multiphase Flows," *Appl. Optics,* Vol. 55 (11), 2892-2903 (2016).

[7] M. Beckstead, K. Puduppakkam, P. Thakre, and V. Yang, "Modeling of Combustion and Ignition of Solid-Propellant Ingredients," *Prog. Energ. Combust.*, Vol. 33(6), 497-551 (2007).

[8] D. Kirchner, J. Gaydos, and M. Battigelli, "Combustion Products of Propellants and Ammunition," in *Occupational Health: The Soldier and the Industrial Base*, D. Deeter, J. Gaydos, eds. (U.S. Dept. of the Army, 1993), pp. 359-396.

[9] Ø. Voie, et al., “Health Effects After Firing Small Arms Comparing Leaded and Unleaded Ammunition," *Inhal. Toxicol.*, Vol. 26 (14), 873-879 (2014).

[10] S. Chaturvedi and P. Dave, "Review: Solid Propellants: AP/HTPB Composite Propellants," *Arab. J. Chem.*, (2014).

[11] E. Dreizin, “Metal-based reactive nanomaterials,” *Prog. Energ. Combust.*, Vol. 35 (2), 141-167 (2009).

[12] S. Chaturvedi and P. Dave, “A review on the use of nanometals as catalysts for the thermal decomposition of ammonium perchlorate,” *J. Saudi Chem. Soc.*, Vol. 17 (2), 135-149 (2013).

[13] V. Arkhipov. and A. Korotkikh, "The Influence of Aluminum Powder Dispersity on Composite Solid Propellants Ignitability by Laser Radiation," *Combust. Flame*, Vol. 159, 409-415 (2012).

[14] L. De Luca, et al., “Burning of Nano-Aluminized Composite Rocket Propellants,” *Combust. Explo. Shock+.*, Vol. 41 (6), 680-692 (2005).

[15] W. Pang, et al, "Effects of Nano-Sized Al on the Combustion Performance of Fuel Rich Solid Rocket Propellants." *Eurasian Chemico-Technological Journal*, Vol. 18 (3), 197-206 (2016).

[16] A. Sossi, et al, "Combustion of HTPB-Based Solid Fuels Loaded with Coated Nanoaluminum," *Combust. Sci. Technol.*, Vol. 185 (1), 17-36 (2013).

[17] J. Moxnes, et al., "Lead Free Ammunition without Toxic Propellant Gases." *Propell. Explos. Pyrot.*, Vol. 38 (2), 255-260 (2013).

[18] N. Andre, et al., "Toxic Potential of Materials at the Nanolevel," *Science*, Vol. 311 (5761), 622-627 (2006).

[19] D. Cremers and L. Radziemski, *Handbook of Laser-Induced Breakdown Spectroscopy*, (John Wiley & Sons, Ltd., 2013).

[20] I. Moench, R. Sattmann, R. Noll, "High-speed identification of polymers by laser-induced breakdown spectroscopy," Proc. SPIE 3100, (1997).

[21] B. Le Drogoff, et al., "Influence of the Laser Pulse Duration on Spectrochemical Analysis of Solids by Laser-Induced Plasma Spectroscopy." *Appl. Spectrosc.*, Vol. 58 (1), 122–129 (2004).

[22] M. Cheng, "Real-Time measurement of trace metals on fine particles by laser-Induced plasma techniques," *Fuel Process. Technol.*, Vol. 65, 219–229 (2000).

[23] R. Vander Wal, T. Ticich, J. West, and P. Householder, "Trace Metal Detection by Laser-Induced Breakdown Spectroscopy," Appl. Spectrosc., Vol. 53, 1226-1236 (1999).

[24] P. Fichet, et al., "Quantitative elemental decomposition in water and oil by laser induced breakdown spectroscopy," *Anal. Chim. Acta*, Vol. 429 (2), 269–278 (2001).

[25] F. Ferioli and S. Buckley, "Measurements of Hydrocarbons Using Laser-Induced Breakdown Spectroscopy," *Combust. Flame*, Vol. 144 (3), 435-447 (2006).

[26] J. Kim, et al., "Instantaneous Monitoring of Local Fuel Concentration in a Liquid Hydrocarbon-Fueled Flame Using a LIBS Plug," *Energy*, Vol. 140, 18-26 (2017).

[27] Y. Zhang, et al., "A New Diagnostic for Volume Fraction Measurement of Metal-Oxide Nanoparticles in Flames Using Phase-Selective Laser-Induced Breakdown Spectroscopy," *P. Combust. Inst.*, Vol. 35 (3), 3681-3688 (2015).

[28] T. Lee and N. Hegde, "Laser-Induced Breakdown Spectroscopy for in Situ Diagnostics of Combustion Parameters Including Temperature," *Combust. Flame*, Vol. 142 (3), 314-316 (2005).

[29] M. O'Neil, "Laser-Induced Breakdown Spectroscopy (LIBS) for Detecting Metal Particles Released from Energetic Reactions," M.S. thesis (Department of Mechanical Engineering, Texas A&M University, 2017).

[30] M. O'Neil, N. Niemiec, A. Demko, E. Petersen, and W. Kulatilaka, "Characterization of Emissions from Metalized Energetic Formulations Using Laser-Induced Breakdown Spectroscopy," in *55th AIAA Aerospace Sciences Meeting, AIAA SciTech Forum*, (AIAA 2017).

[31] R. Adrian, "Particle-Imaging Techniques for Experimental Fluid Mechanics," *Annu. Rev. Fluid Mech.,* Vol. 23 (1), 261-304 (1991).

[32] J. Katz and J. Sheng, "Applications of Holography in Fluid Mechanics and Particle Dynamics," *Annu. Rev. Fluid Mech.*, Vol. 42, 531–555 (2010).

[33] U. Schnars and W. Jueptner, *Digital Holography: Digital Hologram Recording, Numerical Reconstruction, and Related Techniques (Springer, 2005).*

[34] D. Guildenbecher, et al., "Quantitative, Three-Dimensional Imaging of Aluminum Drop Combustion in Solid Propellant Plumes via Digital In-Line Holography," *Opt. Lett.*, Vol. 39 (17), 5126-5129 (2014).

[35] M. Stephens, E. Petersen, R. Carro, D. Reid, and S. Seal, "Multi Parameter Study of Nanoscale TiO2 and CeO2Additives in Composite AP/HTPB Solid Propellants," *Propell. Explos. Pyrot.*, Vol. 35 (2), 143–152 (2010).

[36] M. Stephens, T. Sammet, R. Carro, A. LePage, and E. Petersen, "Comparison of Hand and Mechanically Mixed AP/HTPB SolidComposite Propellants," in *43rd AIAA/ASME/SAE/ASEE Joint Propulsion Conference & Exhibit*, (AIAA, 2007).